Nonconvex mean curvature flow as a formal singular limit of the nonlinear bidomain model

Giovanni Bellettini* Maurizio Paolini† Franco Pasquarelli‡

Abstract

In this paper we study the nonconvex anisotropic mean curvature flow of a hypersurface. This corresponds to an anisotropic mean curvature flow where the anisotropy has a nonconvex Frank diagram. The geometric evolution law is therefore forward-backward parabolic in character, hence ill-posed in general. We study a particular regularization of this geometric evolution, obtained with a nonlinear version of the so-called bidomain model. This is described by a degenerate system of two uniformly parabolic equations of reaction-diffusion type, scaled with a positive parameter ϵ. We analyze some properties of the formal limit of solutions of this system as $\epsilon \to 0^+$, and show its connection with nonconvex mean curvature flow. Several numerical experiments substantiating the formal asymptotic analysis are presented.

1 Introduction

Mean curvature flow, namely the motion of a hypersurface having normal velocity equal to its mean curvature, is the gradient flow of the area functional, and has been the subject of several papers in the last few years, see [12], [28], [21], [29], [30], and the more recent monographs [17], [22], [31] and the references therein. Among the various extensions of this geometric evolution, that has been considered for geometric reasons and also for applications to phase transitions and crystals growth, there is the so-called anisotropic mean curvature flow. In this case, the ambient space $\mathbb{R}^d$ is endowed with a Riemann, or more generally a Finsler [2] metric φ inducing the corresponding distance d_φ. Then anisotropic mean curvature flow is the gradient flow of the φ-anisotropic perimeter functional (called also weigthed area). The integrand of this functional is the dual φ^o of φ weighting the normal directions to the hypersurface, which consequently evolves with velocity along its Cahn-Hoffman direction n^φ equal to its φ-anisotropic mean curvature, see for instance [25], [11], [10]. A sort of limiting case is when φ is polyhedral, and this corresponds to crystalline mean curvature flow, where the mean curvature becomes, in some sense, nonlocal: see [38], [39], [40], [20], [23], [24], [6], [7], [8].

*Dipartimento di Matematica, Università di Roma Tor Vergata, via della Ricerca Scientifica 1, 00133 Roma, Italy, and INFN Laboratori Nazionali di Frascati (LNF), via E. Fermi 40, Frascati 00044 Roma, Italy. E-mail: belletti@mat.uniroma2.it

†Dipartimento di Matematica, Università Cattolica "Sacro Cuore", via Trieste 17, 25121 Brescia, Italy E-mail: paolini@dmf.unicatt.it

‡Dipartimento di Matematica, Università Cattolica "Sacro Cuore", via Trieste 17, 25121 Brescia, Italy E-mail: f.pasquarelli@dmf.unicatt.it

A natural subsequent step in the study of geometric evolutions of hypersurfaces, and which is our main interest in the present paper, is to consider what we can call the *nonconvex mean curvature flow*. This corresponds to an anisotropic mean curvature flow where, however, the unit ball of φ^o (that with a small abuse of language we continue to call Frank diagram, as it is customary in the Finsler case) is *not anymore convex*, but is just a smooth bounded *star-shaped* symmetric[1] set containining the origin in its interior. Here the situation becomes immediately quite intricated: just to mention only a few aspects of the problem, the boundary of the dual body of the Frank diagram has, in general, self-intersections and cusps. In particular, we cannot straightforwardly speak about the distance induced by a norm dual of φ^o. Furthermore, the nonconvexity of φ^o implies that we are considering the gradient flow of a nonconvex (and nonconcave) functional: this leads to a forward-backward parabolic evolution problem, which for a large set of initial data is, in general, ill-posed. From the mathematical point of view, and to our best knowledge, understanding a class of evolving hypersurfaces where reasonably looking for a gradient flow solution in accordance with numerical experiments, is an open problem, as well as a related short time existence result. Taking an initial hypersurface having all normals in the region where φ^o is locally convex, shows that the resulting evolution should not coincide with the anisotropic mean curvature evolution corresponding to the convexified of φ^o. The numerical experiments of [19] (see also [4] in a nongeometric case) obtained by suitable regularization procedures, confirm this assertion. Note, incidentally, that no comparison principle should be expected for nonconvex mean curvature flow, at least in the standard form which is valid for anisotropic and crystalline mean curvature flows.

When facing an ill-posed parabolic problem, a natural idea is to regularize it in some ways, and then try to pass to the limit as the regularization parameter goes to zero, see for instance [36], [35], [16], [19], [18], [4], [37] and references therein. As it happens for forward-backward parabolic equations in one space dimension, various different regularizations are possible, and in principle they could lead to different (subsequential) limits, even for a large class of initial data. In the case of geometric evolutions one possibility is to add to the evolution a higher order term, which for instance in the case of curves ($d = 2$) is usually obtained by computing the first variation of the elastica functional (see [5] for the case of mean curvature flow).

Our interest here is focused on a completely different regularization, coming from the so-called "bidomain model", which provides an approximating problem described by a degenerate system of two uniformly parabolic partial differential equations. The two equations are of reaction-diffusion type in the scalar unknown functions u^{i}_ϵ, u^{e}_ϵ, and the system reads as follows:

$$\begin{cases} \epsilon^2 \partial_t (u^{\mathrm{i}}_\epsilon - u^{\mathrm{e}}_\epsilon) - \epsilon^2 \mathrm{div} T^{\mathrm{i}}(\nabla u^{\mathrm{i}}) + f(u^{\mathrm{i}}_\epsilon - u^{\mathrm{e}}_\epsilon) = 0, \\ \epsilon^2 \partial_t (u^{\mathrm{i}}_\epsilon - u^{\mathrm{e}}_\epsilon) + \epsilon^2 \mathrm{div} T^{\mathrm{e}}(\nabla u^{\mathrm{e}}_\epsilon) + f(u^{\mathrm{i}}_\epsilon - u^{\mathrm{e}}_\epsilon) = 0. \end{cases} \tag{1.1}$$

The function f in the reaction terms is the derivative of a potential W with two minima at equal depth. For definiteness we fix $W(u) := (u^2 - 1)^2$ for $u \in \mathbb{R}$, so that $f(u) = 4u(u^2 - 1)$, see Figure 1.

In system (1.1), $\epsilon > 0$ is a small parameter that will tend to zero, and $T^{\mathrm{i}}, T^{\mathrm{e}} : \mathbb{R}^d \to \mathbb{R}^d$ are

[1] Symmetry of the Frank diagram leads to symmetry of the related distance, which in turn implies that the related anysotropic mean curvature is independent of the choice of the orientation of the flowing hypersurface. The results of this paper hold true also in the nonsymmetric case.

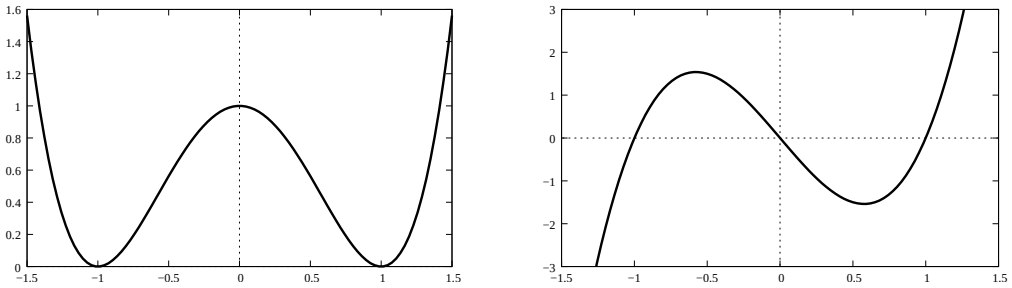

Figure 1: Plot of the potential W (left) and its derivative f (right).

two possibly nonlinear monotone functions defined as

$$T^{\mathrm{i}} = \frac{1}{2}\nabla\alpha^{\mathrm{i}}, \qquad T^{\mathrm{e}} = \frac{1}{2}\nabla\alpha^{\mathrm{e}},$$

where

$$\alpha^{\mathrm{i}}, \alpha^{\mathrm{e}} : \mathbb{R}^d \to [0, +\infty) \tag{1.2}$$

are smooth, *uniformly convex*, and positively homogeneous functions of degree two, i.e.

$$\alpha^{\mathrm{i}}(\mu\xi^\star) = \mu^2\alpha^{\mathrm{i}}(\xi^\star), \quad \alpha^{\mathrm{e}}(\mu\xi^\star) = \mu^2\alpha^{\mathrm{e}}(\xi^\star), \qquad \mu \geq 0,\ \xi^\star \in \mathbb{R}^d, \tag{1.3}$$

and consequently T^{i} and T^{e} are positively homogeneous of degree one[2]. Using the Euler identity for homogeneous functions, the positive two-homogeneity of α^{i} and α^{e} entails

$$\alpha^{\mathrm{i}}(\xi^\star) = \langle \xi^\star, T^{\mathrm{i}}(\xi^\star)\rangle, \quad \alpha^{\mathrm{e}}(\xi^\star) = \langle \xi^\star, T^{\mathrm{e}}(\xi^\star)\rangle, \qquad \xi^\star \in \mathbb{R}^d, \tag{1.4}$$

and

$$T^{\mathrm{i}}(\xi^\star) = M^{\mathrm{i}}(\xi^\star)\xi^\star, \qquad T^{\mathrm{e}}(\xi^\star) = M^{\mathrm{e}}(\xi^\star)\xi^\star, \qquad \xi^\star \in \mathbb{R}^d, \tag{1.5}$$

where $M^{\mathrm{i}}(\xi^\star)$ and $M^{\mathrm{e}}(\xi^\star)$ are symmetric positive definite $(d \times d)$ matrices depending on $\xi^\star$ and positively homogeneous of degree zero, given by

$$M^{\mathrm{i}}(\xi^\star) = (M^{\mathrm{i}}_{hk}(\xi^\star)) \quad \text{with} \quad M^{\mathrm{i}}_{hk}(\xi^\star) = \frac{1}{2}\frac{\partial^2\alpha^{\mathrm{i}}(\xi^\star)}{\partial\xi^\star_h\partial\xi^\star_k} = \frac{\partial T^{\mathrm{i}}_h(\xi^\star)}{\partial\xi^\star_k}, \qquad \xi^\star \in \mathbb{R}^d, \tag{1.6}$$

$$M^{\mathrm{e}}(\xi^\star) = (M^{\mathrm{e}}_{hk}(\xi^\star)) \quad \text{with} \quad M^{\mathrm{e}}_{hk}(\xi^\star) = \frac{1}{2}\frac{\partial^2\alpha^{\mathrm{e}}(\xi^\star)}{\partial\xi^\star_h\partial\xi^\star_k} = \frac{\partial T^{\mathrm{e}}_h(\xi^\star)}{\partial\xi^\star_k}, \qquad \xi^\star \in \mathbb{R}^d. \tag{1.7}$$

Remark 1.1. Symmetry of α^{i} and α^{e}, i.e. $\alpha^{\mathrm{i}}(-\xi^\star) = \alpha^{\mathrm{i}}(\xi^\star)$ and $\alpha^{\mathrm{e}}(-\xi^\star) = \alpha^{\mathrm{e}}(\xi^\star)$ is not required here. However it is useful to keep in mind that a nonsymmetric choice would lead to a notion of anysotropic "norm" φ and "distance" dist_φ (see Section 3.2) that do not satisfy the symmetry property.

To continue our discussion we need the concept of combined anisotropy.

[2]The notation $\xi^\star$ is used to recall that $\xi^\star$ is considered as a covector.

Definition 1.2. *We define Φ, he combined anisotropy of α^{i} and α^{e}, as follows:*

$$\Phi^2 := \left[\frac{1}{\alpha^{\mathrm{i}}} + \frac{1}{\alpha^{\mathrm{e}}}\right]^{-1} = \frac{\alpha^{\mathrm{i}}\alpha^{\mathrm{e}}}{\alpha^{\mathrm{i}} + \alpha^{\mathrm{e}}}. \tag{1.8}$$

We set

$$F_\Phi := \{\xi^\star \in \mathbb{R}^d : \Phi(\xi^\star) \leq 1\},$$

and we call F_Φ the Frank diagram of the combined anisotropy. We also let $T_\Phi := \frac{1}{2}\nabla(\Phi)^2$.

Remark 1.3. A very special situation corresponds to linearly dependent anisotropies, i.e. when α^{e} is a positive multiple of α^{i} (this is called the case of equal anisotropic ratio). In these circumstances system (1.1) reduces (as it can be seen by taking a suitable convex combination of the two equations) to a single reaction-diffusion equation of Allen-Cahn type in the unknown $u^{\mathrm{i}}_\epsilon - u^{\mathrm{e}}_\epsilon$ where the combined anisotropy is itself a factor times α^{i}. The mathematical study is not particularly new in this case, and therefore we will not address the equal anisotropic ratio in the present paper.

Before describing in more details the origin of the bidomain model and hence of system (1.1), it is worthwhile to advise the reader that:

(i) we will distinguish the linear bidomain model from what we will call the *nonlinear bidomain model*. The linear case corresponds to when the maps T^{i} and T^{e} are linear[3], hence α^{i} and α^{e} are two riemannian metrics,

$$\alpha^{\mathrm{i}}(\xi^\star) = \langle M^{\mathrm{i}}\xi^\star, \xi^\star\rangle, \quad \alpha^{\mathrm{e}}(\xi^\star) = \langle M^{\mathrm{e}}\xi^\star, \xi^\star\rangle, \qquad \xi^\star \in \mathbb{R}^d, \tag{1.9}$$

and M^{i}, M^{e} are two symmetric positive definite matrices *independent* of $\xi^\star$. This is a case studied in the literature, and a well-posedness result for system (1.1) is available [15]. We believe the nonlinear case, of which we are not aware about well-posedness results, to be natural for various reasons, that will be made more clear, for instance, in Sections 2 and 3. In the present paper we will be interested in the asymptotic behaviour of solutions u^{i}, u^{e} to system (1.1) as $\epsilon \to 0^+$ also in the nonlinear case.

(ii) Convexity of Φ^2 is *not* guaranteed even in the linear case, and this is indeed the main point of the present paper. The Frank diagram F_Φ of Φ is, indeed, a smooth bounded star-shaped set containing the origin in its interior, and is not necessarily convex. Notice that when it happens that F_Φ is convex, then Φ is in general a Finsler norm, and not necessarily a Riemann one, even when α^{i} and α^{e} are riemannian.

(iii) The result of Section 3 shows that, asymptotically as $\epsilon \to 0^+$, the quantity $u^{\mathrm{i}}_\epsilon - u^{\mathrm{e}}_\epsilon$ has a zero-level set that, approximately, evolves by Φ-anisotropic mean curvature. This is proved here only at a *formal* level, based on matched asymptotic expansions, and assuming uniform convexity and smoothness of Φ. A previous formal result, in the linear case (again valid under the assmption that Φ is uniformly convex and smooth),

[3] T^{i} and T^{e} are in this case linear in the gradient. In the literature they are usually supposed to depend also on the position x, so that $T^{\mathrm{i}} = T^{\mathrm{i}}(x, \nabla u^{\mathrm{i}}(x))$, $T^{\mathrm{e}} = T^{\mathrm{e}}(x, \nabla u^{\mathrm{e}}(x))$, and the two matrices M^{i}, M^{e} in (1.9) depend on the position x. The x-dependence will not be considered in the present paper.

appeared in [3], and one of its consequences is that $u_\epsilon^{\rm i} - u_\epsilon^{\rm e}$ tends to solve a nonlinear single reaction-diffusion equation leading in the limit $\epsilon \to 0^+$ to Φ-anisotropic mean curvature flow (see also Section 5.1 for the nonlinear case). This result has, in some sense, been confirmed from a different perspective in [1]; in this paper the authors showed that system (1.1), in the linear case and for suitable choices of $M^{\rm i}$ and $M^{\rm e}$, is the gradient flow, with respect to a degenerate scalar product, of a sequence of functionals (defined on vector-valued functions) which Γ-converge, as $\epsilon \to 0^+$, to a limit integral functional. The unit ball of the limit integrand is proven *to contain* F_Φ (and therefore its convex hull $\mathrm{co}(F_\Phi)$), and to be *properly contained* in the smallest ellipsoid containing $\mathrm{co}(F_\Phi)$[4].

(iv) Our main numerical simulations in Section 6 are based on a discretization of system (1.1) when Φ is *not* convex, in the linear case and for $d = 2$, thus combining two suitable ellipses (the Frank diagrams of $\alpha^{\rm i}$ and $\alpha^{\rm e}$). A rigorous justification of the convergence of $\{u_\epsilon^{\rm i} - u_\epsilon^{\rm e} = 0\}$ to a nonconvex mean curvature flow is missing, and seems a difficult open problem.

1.1 The bidomain model

We now come to a quick introduction of the (linear) bidomain model, referring to the papers [15], [14] and references therein for the details. The bidomain model for the cardiac tissue originates with the aim of modelling the propagation of the electric signal in the cardiac muscle and of reproducing a complete heartbeat. The myocardium is first considered at a microscopic level as decomposed in an intra-cellular and an extra-cellular domain, where the electric potential is governed through a Poisson equation. The two potentials $u^{\rm i}$ (intra-cellular) and $u^{\rm e}$ (extra-cellular) are coupled at the common interfacial membrane where the difference $u^{\rm i} - u^{\rm e}$ (called transmembrane potential) plays the most importan role. It first varies rapidly during the depolarization phase where it reaches a plateau value s_+; then the (less rapid) repolarization phase allows to recover the basic rest state s_-. The resulting ionic model is governed by the Hodgkin-Huxley formalism [27] and requires also the introduction of a number of so-called gating variables. These can be reduced to a single recovery variable in the FitzHugh-Nagumo simplification, see e.g. [32]. The recovery variable is governed by a simple ODE and is basically only required to model the repolarization phase. However we are mainly interested in the dynamics of the depolarization phase, so that we shall simply neglect the recovery variable. This microscopic model is then locally averaged by using a homogeneization technique (see [14]) leading to a macroscopic model in which the two potentials, now indicated by $u_\epsilon^{\rm i}$ and $u_\epsilon^{\rm e}$, coexist in a common domain Ω representing the cardiac tissue. The (small) quantity $\epsilon > 0$ combines in a nondimensional way the various dimensional physiological constants that characterize the electric properties of the tissue. The complex geometry of the microscopic model, involving the shape of the cells, leads to the presence of a strong anisotropy at the macroscopic level. The anisotropy is described by means of two symmetric positive definite matrices mentioned in item (i) above: $M^{\rm i}$ governes the anisotropy of the intra-cellular potential $u_\epsilon^{\rm i}$, whereas $M^{\rm e}$ refers to the extra-cellular potential $u_\epsilon^{\rm e}$. The two

[4] It is not known whether there is coincidence between the unit ball of the integrand of the Γ-limit and $\mathrm{co}(F_\Phi)$.

matrices have common principal axes aligned with the direction of the longitudinal axis of the cells which are typically quite elongated in shape. The transmembrane potential $u_\epsilon^{\rm i} - u_\epsilon^{\rm e}$ typically exhibits a thin transition region of thickness of order ϵ that separates the advancing depolarized region where $u_\epsilon^{\rm i} - u_\epsilon^{\rm e} \approx s_+$ from the "rest" region where $u_\epsilon^{\rm i} - u_\epsilon^{\rm e} \approx s_-$, $s_- < s_+$ are the two minima of a double-well potential W with $W(s_+) < W(s_-)$ during depolarization. Since we are interested mostly in the curvature effect, we shall however take $W(s_-) = W(s_+)$, see Figure 1. The anisotropy governed by $M^{\rm i}$ and $M^{\rm e}$ is highly space dependent, since the orientation of the myocardium fibers changes from point to point and undergoes approximately a 120 degrees variation between the external boundary and the internal (atrial/ventricular) boundary. As already said in a previous footnote, in this paper we will neglect this dependence, and we will concentrate only on the gradient dependence of $T^{\rm i}$ and $T^{\rm e}$.

Duly motivated, let us address now the nonlinear bidomain model. For a given bounded domain $\Omega \subset \mathbb{R}^d$, $d = 2, 3$ and $\epsilon \in (0, 1]$, we will consider system (1.1), coupled with an initial condition[5] for the difference $u_\epsilon^{\rm i}(\cdot, 0) - u_\epsilon^{\rm e}(\cdot, 0)$ and suitable Dirichlet boundary conditions on $\partial\Omega$ for both $u_\epsilon^{\rm i}$ and $u_\epsilon^{\rm e}$, guaranteeing in particular that $u_\epsilon^{\rm i} - u_\epsilon^{\rm e} = 1 + \mathcal{O}(\epsilon^2)$.

Basing on the results of Section 3, we will numerically analyze the nonconvex Φ-mean curvature flow, mainly in the special case of *inverted anisotropic ratio*. This case is somehow the opposite of the equal anisotropy ratio mentioned in Remark 1.3. In the linear case this corresponds to matrices $M^{\rm i}$ and $M^{\rm e}$ having common principal directions (as in the equal anisotropy assumption) and with eigenvalues $\lambda_1, \lambda_2, \lambda_2$ for $M^{\rm i}$ and correspondingly $\lambda_2, \lambda_1, \lambda_1$ for $M^{\rm e}$ (if $d = 2$ we have respectively λ_1, λ_2 and λ_2, λ_1). In particular we have $M^{\rm i} + M^{\rm e} = \lambda \mathrm{Id}$ with $\lambda := \lambda_1 + \lambda_2$. As we will see in Section 4.1, if the ratio λ_2/λ_1 is sufficiently large this leads to a nonconvex combined anisotropy Φ.

Our numerical experiments will focus in particular on the *wrinkling phenomenon*. Indeed, due to the backward character of the expected limit geometric equation, a sort of instability shows up, resulting in a quick formation of a microstructure[6] in parts of the evolving interface [19]. This is called the wrinkling phenomenon, and has been numerically observed for other regularizations of backward-forward parabolic equations, see for instance [4]. The nature of the wrinkling phenomenon deserves further investigation, as well as a rigorous proof of its existence.

The plan of the paper is the following. In Section 2 we make some remarks on the properties of the combined anisotropy Φ, that will be used throughout the paper, and we give some geometric insight on the construction of the set F_Φ. In Section 3 we perform the matched asymptotic expansion for solutions to system (1.1), by transforming it in an equivalent parabolic-elliptic system (see (3.2)). In Section 4 we focus on the case when Φ is nonconvex, in the inverted anisotropic ratio regime, by explicitly computing examples of nonconvex combined anisotropies. In Section 5 we describe the discrete algorithm concerning system (1.1), that we employ for the numerical simulations. In Section 6 we describe and comment on the results of the numerical experiments, performed with $d = 2$, for the linear bidomain model and in the case of inverted anisotropic ratio.

[5] See [15] for a discussion on the proper boundary and initial conditions for the linear bidomain model.

[6] The observed microstructure profiles are smoothened by the parabolic system (1.1).

2 Remarks on the combined anisotropy

It is interesting to observe how to geometrically construct the Frank diagram of Φ, starting from the Frank diagrams of α^{i} and α^{e}. We shall denote by $\mathcal{S}$ the collection of all subsets of $\mathbb{R}^d$ that are compact, star-shaped[7] and having the origin in their interior. Let F_1, $F_2 \in \mathcal{S}$, Given a unit vector $\nu \in \mathbb{R}^d$ and λ_1, $\lambda_2 \in \mathbb{R}^+$ such that $\lambda_i \nu \in F_i$ we construct the point $\sqrt{\lambda_1^2 + \lambda_2^2}\ \nu$. The set F of the points obtained in this way belongs to $\mathcal{S}$ and we call it the star-shaped combination of F_1 and F_2. If F_1 and F_2 are smooth, then also their star-shaped combination is smooth. When $F_1 = \{\alpha^{\mathrm{i}} \leq 1\}$ and $F_2 = \{\alpha^{\mathrm{e}} \leq 1\}$, for α^{i} and α^{e} as in (1.2), (1.3), then the resulting set F is the Frank diagram F_Φ of the combined anisotropy Φ.
The collection of *convex* sets in $\mathcal{S}$ is *not* closed under star-shaped combination, an explicit example of this fact will be constructed in Section 4 and it would be interesting to characterize those sets in $\mathcal{S}$ that can be obtained as star-shaped combination of two convex sets in $\mathcal{S}$. Note that any *convex* set can be obtained by star-shaped combination of two suitably rescaled copies of itself.
In dimension $d = 2$ it is convenient to represent a set $F \in \mathcal{S}$ as the *inverse polar plot* of some function $\gamma_F = \gamma_F(\theta)$, $\theta \in \mathbb{R}/2\pi\mathbb{Z}$, i.e. $F = \{r(\cos\theta, \sin\theta) : 0 \leq r \leq \frac{1}{\gamma_F(\theta)}\}$. The associated function γ_F satisfies $0 < F_- = \inf_\theta \gamma_F \leq \gamma_F \leq \sup_\theta \gamma_F = F_+$. If F is convex, then it is the Frank diagram of the anisotropy associated to $\varphi^o(\rho(\cos\theta, \sin\theta)) = \rho\gamma_F(\theta)$. Given $F, G \in \mathcal{S}$, the star-shaped combination H of F and G can now be represented by the function

$$\gamma_H(\theta) = \frac{\gamma_F(\theta)\gamma_G(\theta)}{\sqrt{\gamma_F^2(\theta) + \gamma_G^2(\theta)}}.$$

For a *smooth* set $F \in \mathcal{S}$ ($d = 2$) it is well-known that its convexity is equivalent to $\gamma_F + \gamma_F'' \geq 0$. It is convenient to introduce the functions[8]

$$\mathcal{H}_F := \frac{\gamma_F'}{\gamma_F}, \qquad \mathcal{K}_F := \frac{\gamma_F + \gamma_F''}{\gamma_F^3}.$$

In terms of such quantities it is possible to compute $\mathcal{H}_H$ and $\mathcal{K}_H$ for the star-shaped combination H of F and G as

$$\mathcal{H}_H = \frac{\gamma_G^2\mathcal{H}_F + \gamma_F^2\mathcal{H}_G}{\gamma_F^2 + \gamma_G^2}, \qquad \mathcal{K}_H = \mathcal{K}_F + \mathcal{K}_G - 3\frac{(\mathcal{H}_F - \mathcal{H}_G)^2}{\gamma_F^2 + \gamma_G^2} \tag{2.1}$$

If $F \in \mathcal{S}$ is smooth and convex, a direct computation involving the comparison between ∂F and its tangent line at a generic point allows to obtain the estimate

$$\gamma_F^2 + (\gamma_F')^2 \leq F_+^2$$

which together with $\gamma_F \geq F_-$ entails

$$|\mathcal{H}_F| \leq \frac{F_+}{F_-} - 1$$

[7] Throughout the paper, F is *star-shaped* means "F is star-shaped about the origin", i.e. $\mu x \in F$ for all $x \in F$, $\mu \in [0, 1]$.

[8] The euclidean curvature of the boundary is given by $\frac{\gamma+\gamma''}{(1+\mathcal{H}^2)^{3/2}} = \frac{\mathcal{K}}{V^3}$ where $V = \frac{\sqrt{1+\mathcal{H}^2}}{\gamma}$ is the velocity of a point on the boundary moving with unit angular speed.

leading to an upper bound for $|\mathcal{H}_H|$ and lower bound for $\mathcal{K}_H$

$$|\mathcal{H}_H| \leq \frac{G_+^2\left(\frac{F_+}{F_-}-1\right)+F_+^2\left(\frac{G_+}{G_-}-1\right)}{F_-^2+G_-^2}, \qquad \mathcal{K}_H \geq -3\frac{\left(\frac{F_+}{F_-}+\frac{G_+}{G_-}-2\right)^2}{F_-^2+G_-^2}$$

that are uniform with respect to smoothing of a possibly nonregular pair of convex sets F, $G \in \mathcal{S}$, so that they lead to conditions on the star-shaped combination of two generic possibly nonsmooth convex sets in $\mathcal{S}$. The first estimate leads to an internal angle condition with an angle with aperture that depends on the four quantities F_-, F_+, G_-, G_+ and bisector through the origin (thus excluding the presence of cusps pointing outwards), the second leads to an *external tangent ball* condition with a ball having radius that depends on F_-, F_+, G_-, G_+ (thus excluding the presence of reentrant corners).
We can then conclude that $\mathcal{S}_{\text{convex}} \subset \mathcal{S}_{\text{combined}} \subset \mathcal{S}$, with proper inclusions, where $\mathcal{S}_{\text{convex}} = \{F \in \mathcal{S} : F \text{ is convex}\}$ and $\mathcal{S}_{\text{combined}}$ is the collection of the star-shaped combination of two sets in $\mathcal{S}_{\text{convex}}$.

2.1 Representation of the hessian of the combined anisotropy

In Section 3 we will need various representations of the hessian $\nabla^2\Phi$ of Φ, that we present here. A direct computation gives

$$\frac{1}{2}\nabla^2(\Phi^2) = Q + Q_0, \tag{2.2}$$

where

- $Q = Q(\xi^\star)$ takes the form

$$Q = \frac{1}{2}\left(\frac{\alpha^{\mathrm{e}}}{\alpha^{\mathrm{i}}+\alpha^{\mathrm{e}}}\right)^2\nabla^2\alpha^{\mathrm{i}} + \frac{1}{2}\left(\frac{\alpha^{\mathrm{i}}}{\alpha^{\mathrm{i}}+\alpha^{\mathrm{e}}}\right)^2\nabla^2\alpha^{\mathrm{e}} = \left(\frac{\alpha^{\mathrm{e}}}{\alpha^{\mathrm{i}}+\alpha^{\mathrm{e}}}\right)^2 M^{\mathrm{i}} + \left(\frac{\alpha^{\mathrm{i}}}{\alpha^{\mathrm{i}}+\alpha^{\mathrm{e}}}\right)^2 M^{\mathrm{e}}, \tag{2.3}$$

  which can also be written as

$$Q = \Phi^2\left(\frac{M^{\mathrm{i}}}{\alpha^{\mathrm{i}}} + \frac{M^{\mathrm{e}}}{\alpha^{\mathrm{e}}} - \frac{M^{\mathrm{i}}+M^{\mathrm{e}}}{\alpha^{\mathrm{i}}+\alpha^{\mathrm{e}}}\right), \tag{2.4}$$

- $Q_0 = Q_0(\xi^\star)$ depends only on first derivatives of α^{i}, α^{e} and takes the form

$$\begin{aligned} Q_0 = &-\frac{(\alpha^{\mathrm{e}})^2}{(\alpha^{\mathrm{i}}+\alpha^{\mathrm{e}})^3}\nabla\alpha^{\mathrm{i}}\otimes\nabla\alpha^{\mathrm{i}} - \frac{(\alpha^{\mathrm{i}})^2}{(\alpha^{\mathrm{i}}+\alpha^{\mathrm{e}})^3}\nabla\alpha^{\mathrm{e}}\otimes\nabla\alpha^{\mathrm{e}} \\ &+ \frac{2\alpha^{\mathrm{i}}\alpha^{\mathrm{e}}}{(\alpha^{\mathrm{i}}+\alpha^{\mathrm{e}})^3}\nabla\alpha^{\mathrm{i}}\otimes\nabla\alpha^{\mathrm{e}} = -\frac{w\otimes w}{(\alpha^{\mathrm{i}}+\alpha^{\mathrm{e}})^3}, \end{aligned}$$

  where $w = w(\xi^\star)$ reads as $w = \alpha^{\mathrm{i}}\nabla\alpha^{\mathrm{e}} - \alpha^{\mathrm{e}}\nabla\alpha^{\mathrm{i}}$. Notice that

$$\langle w(\xi^\star), \xi^\star\rangle = 0, \qquad \xi^\star \in \mathbb{R}^d, \tag{2.5}$$

  since $\langle w(\xi^\star), \xi^\star\rangle = \alpha^{\mathrm{i}}(\xi^\star)\alpha^{\mathrm{e}}(\xi^\star) - \alpha^{\mathrm{e}}(\xi^\star)\alpha^{\mathrm{i}}(\xi^\star)$, as a consequence of (1.4).

From (2.2) and (2.5) we obtain the following representation:

$$T_\Phi(\xi^\star) = Q(\xi^\star)\xi^\star, \qquad \xi^\star \in \mathbb{R}^d. \tag{2.6}$$

In terms of $Q(\cdot)$, which is homogeneous of degree zero, we can also recover the following alternative representation of Φ:

$$\Phi(\xi^\star) = \sqrt{\langle \xi^\star, Q(\xi^\star)\xi^\star \rangle}, \qquad \xi^\star \in \mathbb{R}^d.$$

Remark 2.1. We stress that, in view of its dependence on $\xi^\star$, matrix $Q(\xi^\star)$ is *not* uniquely defined by relation (2.6), even among symmetric positive definite matrices. Indeed the Hessian of $\frac{1}{2}\Phi^2(\xi^\star)$ provides another (and perhaps more natural) matrix $M^c(\xi^\star)$ satisfying (2.6). It differs from Q by $Q_0 = M^c - Q$. It is a matrix of rank one having $\xi^\star$ in its kernel.

2.2 Notation when Φ is convex

When Φ is convex, we define the function $\varphi : \mathbb{R}^d \to [0, +\infty)$ as the dual Φ^o of Φ, therefore by the convexity assumption $\Phi = \varphi^o$ and $\varphi := \varphi^{oo}$. We denote by $\mathrm{dist}_\varphi(x, y) := \varphi(y - x)$ the associated anisotropic distance between the two points $x, y \in \mathbb{R}^d$, and $\mathrm{dist}_\varphi(x, E) := \inf\{\mathrm{dist}_\varphi(x, y) : y \in E\}$ the anisotropic distance of a point $x \in \mathbb{R}^d$ from a set $E \subseteq \mathbb{R}^d$. We also set

$$T^o = T_\Phi. \tag{2.7}$$

Notice that viewing in this case Φ as a dual justifies the use of the notation $\xi^\star$ to indicate its argument, which indeed should be considered as a covector, namely an element of the dual of $\mathbb{R}^d$.

3 Matched asymptotics for the nonlinear bidomain model

In this section we perform a formal matched asymptotic expansion for the *nonlinear* bidomain model; we will follow the computations made in [3] for the linear case[9], writing the parabolic nonlinear system as an equivalent nonlinear parabolic-elliptic system. As we shall see, the nonlinearities of T^{i} and T^{e} are source of various difficulties, so that the final result cannot be deduced from [3]. Differently with respect to the linear case, we will make the computations only up to the first order; a complete formal asymptotic analysis of this model, and of its generalizations to arbitrary dimensions and to an arbitrary number of phases, will appear elsewhere. The outcoming relevant result is that the nonlinear bidomain model formally approximate the (convex and nonconvex) anisotropic mean curvature flow. It is worthwhile to notice that various algebraic relations that we will use in the computations[10] show that the extension of the linear bidomain model to the nonlinear case is rather natural.
Due to the strong reaction term we expect the difference $u^{\mathrm{i}}_\epsilon(\cdot, t) - u^{\mathrm{e}}_\epsilon(\cdot, t)$ to assume values near the two minima ± 1 of the potential W (indicating the two phases $\Omega^-(t)$ and $\Omega^+(t)$) in most of the domain with a thin, smooth, transition region between the two phases where

[9] In [3] a double well potential with wells at different depth is considered, which gives an additional term to the normal velocity of the interface. In the present paper we are concerned with a different scaling of the equations, with respect to [3].

[10] See for instance (3.18), (3.23).

it transversally crosses the unstable zero $u = 0$ of f. This motivates the use of matched asymptotics in the outer $\Omega^-(t) \cup \Omega^+(t)$ region (outer expansion) and in the transition layer (inner expansion). As a consequence, at least formally, the front generated by (1.1) propagates with the same law as the front generated by an anisotropic mean curvature flow, with the combined anisotropy.

Taking the difference of the two equations in (1.1) gives $\mathrm{div}\Big(T^{\mathrm{i}}(\nabla u_\epsilon^{\mathrm{i}}) + T^{\mathrm{e}}(\nabla u_\epsilon^{\mathrm{e}})\Big) = 0$, which can be rewritten in terms of

$$u_\epsilon := u_\epsilon^{\mathrm{i}} - u_\epsilon^{\mathrm{e}}, \qquad w_\epsilon := u_\epsilon^{\mathrm{i}} \tag{3.1}$$

as $\mathrm{div}\Big(T^{\mathrm{i}}(\nabla w_\epsilon) + T^{\mathrm{e}}(\nabla w_\epsilon - \nabla u_\epsilon)\Big) = 0$. We end up with the equivalent formulation

$$\begin{cases} \epsilon^2 \partial_t u_\epsilon - \epsilon^2 \mathrm{div}\Big(T^{\mathrm{i}}(\nabla w_\epsilon)\Big) + f(u_\epsilon) = 0 \\ \mathrm{div}\Big(T^{\mathrm{i}}(\nabla w_\epsilon) + T^{\mathrm{e}}(\nabla w_\epsilon - \nabla u_\epsilon)\Big) = 0. \end{cases} \tag{3.2}$$

3.1 Outer expansion

Expand formally u_ϵ and w_ϵ in terms of ϵ as $u_\epsilon = u_0 + \epsilon u_1 + \epsilon^2 u_2 + ...$, $w_\epsilon = w_0 + \epsilon w_1 + \epsilon^2 w_2 + ...$ Substituting these expressions into the parabolic equation in (3.2) and using the expansion $f(u_\epsilon) = f(u_0) + \epsilon f'(u_0)u_1 + \epsilon^2 \left(\frac{u_1^2 f''(u_0)}{2} + f'(u_0)u_2\right) + \mathcal{O}(\epsilon^3)$ we get $f(u_0) = 0$ and $u_1 f'(u_0) = 0$. Hence, excluding $u_0 = 0$ (the unstable zero of f), we obtain

$$u_0 \equiv 1 \text{ or } u_0 \equiv -1, \qquad u_1 \equiv 0,$$

and therefore

$$u_2 = \frac{1}{f'(u_0)} \mathrm{div}\Big(T^{\mathrm{i}}(\nabla w_0)\Big). \tag{3.3}$$

Using the elliptic equation in (3.2) we find

$$\mathrm{div}\Big(T^{\mathrm{i}}(\nabla w_0) + T^{\mathrm{e}}(\nabla w_0)\Big) = 0. \tag{3.4}$$

This is, in general, a nonlinear elliptic equation (to be considered with suitable Dirichlet boundary conditions on $\partial\Omega$); the boundary conditions across the limit interface to be coupled with (3.4) will arise by matching the outer expansion with the inner expansion, see (3.33) and (3.34) (jump condition and jump of the normal derivative of w_0, respectively). We assume this elliptic problem to be solvable, thus providing w_0 and therefore u_2 from (3.3). By using a Taylor expansion of T^{i} and T^{e}, namely

$$\begin{aligned} T^{\mathrm{i}}(\eta^\star + \epsilon\zeta^\star) &= T^{\mathrm{i}}(\eta^\star) + \epsilon M^{\mathrm{i}}(\eta^\star)\zeta^\star + \mathcal{O}(\epsilon^2), \\ T^{\mathrm{e}}(\eta^\star + \epsilon\zeta^\star) &= T^{\mathrm{e}}(\eta^\star) + \epsilon M^{\mathrm{e}}(\eta^\star)\zeta^\star + \mathcal{O}(\epsilon^2), \end{aligned} \tag{3.5}$$

a computation gives

$$\mathrm{div}\Big(\big(M^{\mathrm{i}}(\nabla w_0) + M^{\mathrm{e}}(\nabla w_0)\big)\nabla w_1\Big) = 0,$$

which is a linear elliptic equation in w_1, that we do not need to inspect.

Remark 3.1. Notice that the outer expansion has been performed without assuming that Φ is convex.

3.2 Inner expansion

We assume in this section that Φ is uniformly convex (and smooth): therefore we can employ the notation introduced in Section 2.2, in particular Φ equals the dual φ^o of a convex norm φ and $T^o = T_\Phi$, dist_φ is the anisotropic distance associated with φ, $d^\varphi_\epsilon(x,t) := \mathrm{dist}_\varphi(x, \mathbb{R}^d \setminus E_\epsilon(t)) - \mathrm{dist}_\varphi(x, E_\epsilon(t))$ is the signed distance function from $E_\epsilon(t)$ positive in $E_\epsilon(t)$ where, recalling the definition of u_ϵ in (3.1), we let

$$E_\epsilon(t) := \{x \in \Omega : u_\epsilon(x,t) \geq 0\}.$$

For notational simplicity we set $\Sigma_\epsilon(t) := \partial E_\epsilon(t) = \{x \in \Omega : u_\epsilon(x,t) = 0\}$.
Our aim is to formally identify the geometric evolution law of $\Sigma_\epsilon(t)$ as $\epsilon \to 0^+$. To this aim it is convenient to introduce the stretched variable y_ϵ, defined as $y^\varphi_\epsilon(x,t) := \frac{d^\varphi_\epsilon(x,t)}{\epsilon}$.
We parametrize $\Sigma_\epsilon(t)$ with a parameter s which varies in a fixed reference $(d-1)$-dimensional smooth manifold of fixed topological type, and the function $x(s,t;\epsilon)$ gives the position in Ω of the point s at time t. We let, for x in a suitable tubular neighbourhood of $\Sigma_\epsilon(t)$, $n^\varphi_\epsilon(x,t) := -T^o(\nabla d^\varphi_\epsilon(x,t))$ be the Cahn-Hoffman vector field (pointing toward $\mathbb{R}^d \setminus E_\epsilon(t)$)), for which we suppose the expansion $n^\varphi_\epsilon := n^\varphi_0 + \epsilon n^\varphi_1 + ...$
Points on the evolving manifold $\Sigma_\epsilon(t)$ are assumed to move in the direction of $n^\varphi_\epsilon(\cdot,t)$, i.e.,

$$\partial_t x(s,t;\epsilon) = V^\varphi_\epsilon \; n^\varphi_\epsilon,$$

where V_ϵ is conventionally positive for an expanding set, and where we assume the validity of the expansion $V^\varphi_\epsilon = V_0 + \epsilon V_1 + \epsilon^2 V_2 + ...$ The anisotropic projection of a point x on $\Sigma_\epsilon(t)$ will be denoted by $s^\varphi_\epsilon(x,t)$, which satisfies

$$\partial_t s^\varphi_\epsilon = 0. \tag{3.6}$$

Hence

$$\partial_t d^\varphi_\epsilon(x,t) = V^\varphi_\epsilon(s^\varphi_\epsilon(x,t),t). \tag{3.7}$$

We also recall (see [11], [10]) that the φ-anisotropic laplacian of d^φ_ϵ corresponds to the anisotropic mean curvature of the level hypersurface at that point and that it can be approximated by the anisotropic mean curvature κ^φ_ϵ of $\Sigma_\epsilon(t)$ (positive when $E_\epsilon(t)$ is uniformly convex) as follows

$$\mathrm{div}\,(T^o(\nabla d^\varphi_\epsilon(x,t))) = -\kappa^\varphi_\epsilon(s^\varphi_\epsilon(x,t),t) - \epsilon y^\varphi_\epsilon h^\varphi_\epsilon(s^\varphi_\epsilon(x,t),t) + \mathcal{O}(\epsilon^2 (y^\varphi_\epsilon)^2) \tag{3.8}$$

for a suitable h^φ_ϵ depending on the local shape of $\Sigma_\epsilon(t)$, which we do not need to specify. We assume the expansions $\kappa^\varphi_\epsilon = \kappa_0 + \epsilon\kappa_1 + \mathcal{O}(\epsilon^2)$, $h^\varphi_\epsilon = h_0 + \mathcal{O}(\epsilon)$. For notational simplicity, in the sequel of this section we shall drop the superscript φ in d_ϵ, y_ϵ, s_ϵ, κ_ϵ and h_ϵ. With abuse of notation, for a given ϵ, we let $x(y;s,t)$ be the point of Ω having signed distance ϵy and φ-anisotropic projection s on $\Sigma_\epsilon(t)$. We have

$$x(y;s,t) = x(s,t) - \epsilon y n^\varphi_\epsilon + \mathcal{O}(\epsilon^2 y^2). \tag{3.9}$$

For a given ϵ the triplet $(y;s,t)$ will parametrize a tubular neighbourhood of $\cup_t(\Sigma_\epsilon(t) \times \{t\})$. We define $U_\epsilon(y;s,t)$ and $W_\epsilon(y;s,t,x)$ so that

$$u_\epsilon(x,t) = U_\epsilon(d_\epsilon(x,t)/\epsilon, s_\epsilon(x,t), t), \qquad w_\epsilon(x,t) = W_\epsilon(d_\epsilon(x,t)/\epsilon, s_\epsilon(x,t), t, x).$$

We find convenient, as in [3], to allow W_ϵ to explicitly depend on the "outer" variable x (of course implicit dependence on x is given through y and s). As a notation, when we differentiate W_ϵ using one of the symbols ∇, div, or ∇^2, we mean that only partial derivative of W_ϵ with respect to the x variable is considered.
We will write $W_\epsilon = W_0 + \epsilon W_{1,\epsilon} = W_0 + \epsilon W_1 + \epsilon^2 W_{2,\epsilon}$, where W_0 and W_1 are allowed to depend explicitly on x (and hence on ϵ) in the same way as W_ϵ. We suppose the remainders $W_{1,\epsilon}$, $W_{2,\epsilon}$ to be bounded as $\epsilon \to 0^+$. We adopt a similar notation for $U_\epsilon = U_0 + \epsilon U_{1,\epsilon} = U_0 + \epsilon U_1 + \epsilon^2 U_{2,\epsilon}$, where however we require U_0 not to depend on ϵ.
We have

$$\epsilon^2 \partial_t u_\epsilon = \epsilon U'_\epsilon \ \partial_t d_\epsilon + \epsilon^2 U_{\epsilon s_\beta} \ \partial_t s_{\epsilon\beta} + \epsilon^2 U_{\epsilon t} = \epsilon U'_\epsilon V_\epsilon + \epsilon^2 U_{\epsilon t},$$

where we use (3.6) and (3.7) and summation on repeated indices is understood. Furthermore[11]

$$\begin{aligned} \epsilon^2 T^{\rm i}(\nabla w_\epsilon) =& T^{\rm i}\left(\epsilon W'_\epsilon \nabla d_\epsilon + \epsilon^2 W_{\epsilon s_\beta} \nabla s_{\epsilon\beta} + \epsilon^2 \nabla W_\epsilon\right) \\ =& \epsilon W'_\epsilon \ T^{\rm i}(\nabla d_\epsilon) + \epsilon^2 W_{\epsilon s_\beta} M^{\rm i}(\nabla d_\epsilon) \nabla s_{\epsilon\beta} + \epsilon^2 M^{\rm i}(\nabla d_\epsilon) \nabla W_\epsilon + \mathcal{O}(\epsilon^3), \end{aligned} \tag{3.10}$$

and similarly, recalling that U_ϵ does not depend explicitly on x,

$$\begin{aligned} \epsilon^2 T^{\rm e}(\nabla w_\epsilon - \nabla u_\epsilon) =& T^{\rm e}\Big(\epsilon(W'_\epsilon - U'_\epsilon)\nabla d_\epsilon + \epsilon^2 (W_{\epsilon s_\beta} - U_{\epsilon s_\beta}) \nabla s_{\epsilon\beta} + \epsilon^2 \nabla W_\epsilon\Big) \\ =& \epsilon(W'_\epsilon - U'_\epsilon) T^{\rm e}(\nabla d_\epsilon) + \epsilon^2 (W_{\epsilon s_\beta} - U_{\epsilon s_\beta}) M^{\rm e}(\nabla d_\epsilon) \nabla s_{\epsilon\beta} \\ & + \epsilon^2 M^{\rm e}(\nabla d_\epsilon) \nabla W_\epsilon + \mathcal{O}(\epsilon^3). \end{aligned} \tag{3.11}$$

Taking into account (see (1.5)) that $\langle \nabla s_{\epsilon\beta}, T^{\rm i}(\nabla d_\epsilon)\rangle = \langle \nabla d_\epsilon, M^{\rm i}(\nabla d_\epsilon) \nabla s_{\epsilon\beta}\rangle$, and that[12]

$$\epsilon^2 {\rm div}\Big(M^{\rm i}(\nabla d_\epsilon)\nabla W_\epsilon\Big) = \epsilon \langle \nabla W'_\epsilon, T^{\rm i}(\nabla d_\epsilon)\rangle + \epsilon^2 F,$$

we now differentiate (3.10) and we obtain, using also (1.4),

$$\begin{aligned} &\epsilon^2 {\rm div} T^{\rm i}(\nabla w_\epsilon) = \alpha^{\rm i}(\nabla d_\epsilon) W''_\epsilon + 2\epsilon W'_{\epsilon s_\beta} \langle \nabla s_{\epsilon\beta}, T^{\rm i}(\nabla d_\epsilon)\rangle + 2\epsilon \langle \nabla W'_\epsilon, T^{\rm i}(\nabla d_\epsilon)\rangle \\ &+ \epsilon W'_\epsilon {\rm div}(T^{\rm i}(\nabla d_\epsilon)) + \epsilon^2 W_{\epsilon s_\beta s_\delta} \langle \nabla s_{\epsilon\delta},\ M^{\rm i}(\nabla d_\epsilon)\nabla s_{\epsilon\beta}\rangle + \epsilon^2 \langle \nabla W_{\epsilon s_\beta}, M^{\rm i}(\nabla d_\epsilon)\nabla s_{\epsilon\beta}\rangle \\ &+ \epsilon^2 W_{\epsilon s_\beta} {\rm div}\left(M^{\rm i}(\nabla d_\epsilon)\nabla s_{\epsilon\beta}\right) + \epsilon^2 F + \mathcal{O}(\epsilon^3). \end{aligned}$$

Differentiating (3.11), and taking into account that[13]

$$\epsilon^2 {\rm div}(M^{\rm e}(\nabla d_\epsilon)\nabla W_\epsilon) = \epsilon \langle \nabla W'_\epsilon, T^{\rm i}(\nabla d_\epsilon)\rangle + \epsilon^2 G,$$

we obtain

$$\begin{aligned} &\epsilon^2 {\rm div} T^{\rm e}(\nabla w_\epsilon - \nabla u_\epsilon) \\ =& \alpha^{\rm e}(\nabla d_\epsilon)(W''_\epsilon - U''_\epsilon) + 2\epsilon(W'_{\epsilon s_\beta} - U'_{\epsilon s_\beta}) \langle \nabla s_{\epsilon\beta}, T^{\rm e}(\nabla d_\epsilon)\rangle + 2\epsilon \langle \nabla W'_\epsilon, T^{\rm e}(\nabla d_\epsilon)\rangle \\ &+ \epsilon(W'_\epsilon - U'_\epsilon) {\rm div}(T^{\rm e}(\nabla d_\epsilon)) + \epsilon^2 (W_{\epsilon s_\beta s_\delta} - U_{\epsilon s_\beta s_\delta}) \langle \nabla s_{\epsilon\delta}, M^{\rm e}(\nabla d_\epsilon)\nabla s_{\epsilon\beta}\rangle \\ &+ \epsilon^2 \langle \nabla W_{\epsilon s_\beta}, M^{\rm e}(\nabla d_\epsilon)\nabla s_{\epsilon\beta}\rangle \\ &+ \epsilon^2 (W_{\epsilon s_\beta} - U_{\epsilon s_\beta}) {\rm div}(M^{\rm e}(\nabla d_\epsilon)\nabla s_{\epsilon\beta}) + \epsilon^2 G + \mathcal{O}(\epsilon^3). \end{aligned}$$

[11] Use (3.5), and remember that $M^{\rm i}$ is zero-homogeneous, so that $M^{\rm i}(W'_\epsilon \nabla d_\epsilon) = M^{\rm i}(\nabla d_\epsilon)$.
[12] We use once more (1.5); do not need to explicitate the term F in our subsequent computations.
[13] We do not need to explicitate the term G in our subsequent computations.

In terms of U_ϵ and W_ϵ the expansion of the parabolic equation in (3.2) reads as

$$\begin{aligned}0 =& -\alpha^{\mathrm{i}}(\nabla d_\epsilon)W_\epsilon'' + f(U_\epsilon)\\ &+\epsilon\Big(V_\epsilon U_\epsilon' - 2W'_{\epsilon s_\beta}\langle\nabla s_{\epsilon\beta}, T^{\mathrm{i}}(\nabla d_\epsilon)\rangle - 2\langle\nabla W_\epsilon', T^{\mathrm{i}}(\nabla d_\epsilon)\rangle - W_\epsilon'\mathrm{div}T^{\mathrm{i}}(\nabla d_\epsilon)\Big)\\ &+\epsilon^2\Big(U_{\epsilon t} - W_{\epsilon s_\beta s_\delta}\langle\nabla s_{\epsilon\delta}, M^{\mathrm{i}}(\nabla d_\epsilon)\nabla s_{\epsilon\beta}\rangle - \langle\nabla W_{\epsilon s_\beta}, M^{\mathrm{i}}(\nabla d_\epsilon)\nabla s_{\epsilon\beta}\rangle\\ &\qquad - W_{\epsilon,s_\beta}\mathrm{div}(M^{\mathrm{i}}(\nabla d_\epsilon)\nabla s_{\epsilon\beta}) - F\Big) + \mathcal{O}(\epsilon^3),\end{aligned} \tag{3.12}$$

and the expansion of the elliptic equation in (3.2) reads as

$$\begin{aligned}0 =&\big(\alpha^{\mathrm{i}}(\nabla d_\epsilon) + \alpha^{\mathrm{e}}(\nabla d_\epsilon)\big)W_\epsilon'' - \alpha^{\mathrm{e}}(\nabla d_\epsilon)U_\epsilon''\\ &+\epsilon\Bigg(2W'_{\epsilon s_\beta}\langle\nabla s_{\epsilon\beta}, T^{\mathrm{i}}(\nabla d_\epsilon) + T^{\mathrm{e}}(\nabla d_\epsilon)\rangle - 2U'_{\epsilon s_\beta}\langle\nabla s_{\epsilon\beta}, T^{\mathrm{e}}(\nabla d_\epsilon)\rangle\\ &+2\langle\nabla W_\epsilon', T^{\mathrm{i}}(\nabla d_\epsilon) + T^{\mathrm{e}}(\nabla d_\epsilon)\rangle + W_\epsilon'\mathrm{div}\Big(T^{\mathrm{i}}(\nabla d_\epsilon) + T^{\mathrm{e}}(\nabla d_\epsilon)\Big) - U_\epsilon'\mathrm{div}T^{\mathrm{e}}(\nabla d_\epsilon)\Bigg)\\ &+\epsilon^2\Bigg(W_{\epsilon s_\beta s_\delta}\langle\nabla s_{\epsilon\delta}, \Big(M^{\mathrm{i}}(\nabla d_\epsilon) + M^{\mathrm{e}}(\nabla d_\epsilon)\Big)\nabla s_{\epsilon\beta}\rangle - U_{\epsilon s_\beta s_\delta}\langle\nabla s_{\epsilon\delta}, M^{\mathrm{e}}(\nabla d_\epsilon)\nabla s_{\epsilon\beta}\rangle\\ &+\nabla W_{\epsilon s_\beta}\Big(M^{\mathrm{i}}(\nabla d_\epsilon) + M^{\mathrm{e}}(\nabla d_\epsilon)\Big)\nabla s_{\epsilon\beta} + W_{\epsilon s_\beta}\mathrm{div}\Big(\big(M^{\mathrm{i}}(\nabla d_\epsilon) + M^{\mathrm{e}}(\nabla d_\epsilon)\big)\nabla s_{\epsilon\beta}\Big)\\ &-U_{\epsilon s_\beta}\mathrm{div}\Big(M^{\mathrm{e}}(\nabla d_\epsilon)\nabla s_{\epsilon\beta}\Big) + F + G\Bigg) + \mathcal{O}(\epsilon^3).\end{aligned} \tag{3.13}$$

As we have already mentioned at the beginning of this section, we will not make the computations at the order two: therefore, the coefficients of ϵ^2 in equations (3.12) and (3.13) are given for completeness, and for consistency with the linear case discussed in [3].

3.3 Matching with the outer expansion and formal conclusions

The matching procedure is not necessary for functions U_i, since they are uniquely determined at infinity by a polynomial growth requirement. Therefore, we shall match the inner/outer asymptotic expansions for the functions W_i. We will make use of the change of variables (3.9), and we will match the two expansions in the region of common validity $y \to \infty$ and x approaching $\Sigma_\epsilon(t)$:

$$w_\epsilon(x(s,t) - \epsilon y n_\epsilon^\varphi + \mathcal{O}(\epsilon^2 y^2), t) \approx W_\epsilon(y; s, t, x(s,t) - \epsilon y n_\epsilon^\varphi + \mathcal{O}(\epsilon^2 y^2)).$$

By expanding the left and right hand sides, understanding that w_ϵ is computed at $x(s,t) \in \Sigma_\epsilon(t)$, we get

$$w_\epsilon - \epsilon y\langle n_\epsilon^\varphi, \nabla w_\epsilon\rangle + \mathcal{O}(\epsilon^2) \approx W_\epsilon - \epsilon y\langle n_\epsilon^\varphi, \nabla W_\epsilon\rangle + \mathcal{O}(\epsilon^2).$$

Expanding w_ϵ, W_ϵ, and in powers of ϵ and matching the first two orders we get in particular

$$\begin{aligned}&\lim_{y\to\pm\infty} W_0(y, s(x,t), t, x) = w_0(x,t)\\ &\lim_{y\to\pm\infty}\big\{W_1(y, s(x,t), t, x) - w_1(x,t) - y(\langle n_0^\varphi, \nabla W_0(y, s(x,t), t, x)\rangle - \langle n_0^\varphi, \nabla w_0(x,t))\rangle\big\} = 0\end{aligned} \tag{3.14}$$

where w_i are evaluated at each side of the interface[14] accordingly to when y goes to plus or minus infinity. The first relation in (3.14) in particular suggests $\lim_{y\to\pm\infty} W_0'(y, s(x,t), t, x) = 0$, and the jump $[\![w_0]\!]$ of w_0 across the interface is given by

$$[\![w_0]\!](s(x,t),t) = \int_{\mathbb{R}} W_0'(y, s(x,t), t, x)\ dy. \tag{3.15}$$

By differentiating the second equation in (3.14) we get

$$\begin{aligned}&\lim_{y\to\pm\infty} \big\{W_1'(y, s(x,t), t, x) - \langle n_0^\varphi, \nabla W_0(y, s(x,t), t, x)\rangle - y\langle n_0^\varphi, \nabla W_0'(y, s(x,t), t, x)\rangle\big\}\\ &= -\langle n_0^\varphi, \nabla w_0(x,t)\rangle.\end{aligned} \tag{3.16}$$

After identification of W_0' given by relation (3.20) below, it will also follow (see in addition (3.22)) that also $\lim_{y\to\pm\infty}(y\nabla W_0'(y, s(x,t), t, x)) = 0$ and that $\nabla W_0(y, s(x,t), t, x)$ is bounded, so that W_1' is also bounded and

$$-[\![\langle n_0^\varphi, \nabla w_0\rangle]\!](x,t) = \int_{\mathbb{R}} \big(W_1''(y, s(x,t), t, x) - \langle n_0^\varphi, \nabla W_0'(y, s(x,t), t, x)\rangle\big)\ dy. \tag{3.17}$$

• **Order 0**. Recall that ∇d_ϵ satisfies the anisotropic eikonal equation [10], [3]:

$$\frac{\alpha^{\mathrm{i}}(\nabla d_\epsilon(x,t))\alpha^{\mathrm{e}}(\nabla d_\epsilon(x,t))}{\alpha^{\mathrm{i}}(\nabla d_\epsilon(x,t)) + \alpha^{\mathrm{e}}(\nabla d_\epsilon(x,t))} = \Big(\Phi(\nabla d_\epsilon(x,t))\Big)^2 = 1, \tag{3.18}$$

for x in a suitable tubular neighbourhood of $\Sigma_\epsilon(t)$.
Collecting the zero order terms[15] in (3.13) gives $\Big(\alpha^{\mathrm{i}}(\nabla d_\epsilon) + \alpha^{\mathrm{e}}(\nabla d_\epsilon)\Big)W_0'' - \alpha^{\mathrm{e}}(\nabla d_\epsilon)U_0'' = 0$. Hence, using (3.18), we have

$$W_0'' = \frac{\alpha^{\mathrm{e}}(\nabla d_\epsilon)}{\alpha^{\mathrm{i}}(\nabla d_\epsilon) + \alpha^{\mathrm{e}}(\nabla d_\epsilon)} U_0'' = \frac{1}{\alpha^{\mathrm{i}}(\nabla d_\epsilon)} U_0''. \tag{3.19}$$

Since U_0 (see below) and W_0 are bounded at infinity we also get by integration

$$W_0' = \frac{1}{\alpha^{\mathrm{i}}(\nabla d_\epsilon)} U_0'. \tag{3.20}$$

Using the expansion $f(U_\epsilon) = f(U_0) + \epsilon U_{1,\epsilon} f'(U_0) + \frac{1}{2}\epsilon^2 (U_{1,\epsilon})^2 f''(U_0) + \mathcal{O}(\epsilon^3)$, from (3.12) we get $-\alpha^{\mathrm{i}}(\nabla d_\epsilon)W_0'' + f(U_0) = 0$. Our substitution in (3.19) gives

$$-U_0'' + f(U_0) = 0, \tag{3.21}$$

so that

$$U_0(y,s,t) = \gamma(y) := \mathrm{tgh}(\sqrt{2}y), \tag{3.22}$$

and therefore U_0 does not depend on (s,t). Note that W_0' will depend explicitly on x through the coefficient $\frac{1}{\alpha^{\mathrm{i}}(\nabla d_\epsilon)}$; it is, on the other hand, independent of (s,t).

[14] Here by interface we mean the jump set of u_0.

[15] There is no need of expanding d_ϵ in terms of ϵ, since we are taking a reference system based on the zero level sets of $u_\epsilon^{\mathrm{i}} - u_\epsilon^{\mathrm{e}}$.

• **Order 1**. Differentiating the eikonal equation (3.18) with respect to x we obtain

$$0 = \nabla \frac{1}{\alpha^{\mathrm{i}}(\nabla d_\epsilon)} + \nabla \frac{1}{\alpha^{\mathrm{e}}(\nabla d_\epsilon)}, \tag{3.23}$$

which allows to express $\nabla \frac{1}{\alpha^{\mathrm{e}}} = -\nabla \frac{1}{\alpha^{\mathrm{i}}}$. Moreover using (2.6), (2.4) and (3.18) we get

$$\begin{aligned} T^o(\nabla d_\epsilon) =& \frac{1}{\alpha^{\mathrm{i}}(\nabla d_\epsilon)} T^{\mathrm{i}}(\nabla d_\epsilon) + \frac{1}{\alpha^{\mathrm{e}}(\nabla d_\epsilon)} T^{\mathrm{e}}(\nabla d_\epsilon) \\ & - \frac{1}{\alpha^{\mathrm{i}}(\nabla d_\epsilon) + \alpha^{\mathrm{e}}(\nabla d_\epsilon)} \Big(T^{\mathrm{i}}(\nabla d_\epsilon) + T^{\mathrm{e}}(\nabla d_\epsilon) \Big), \end{aligned} \tag{3.24}$$

and therefore

$$\begin{aligned} \mathrm{div} T^o(\nabla d_\epsilon) =& \mathrm{div} \frac{1}{\alpha^{\mathrm{i}}(\nabla d_\epsilon)} T^{\mathrm{i}}(\nabla d_\epsilon) + \mathrm{div} \frac{1}{\alpha^{\mathrm{e}}(\nabla d_\epsilon)} T^{\mathrm{e}}(\nabla d_\epsilon) \\ & - \mathrm{div} \left(\frac{1}{\alpha^{\mathrm{i}}(\nabla d_\epsilon) + \alpha^{\mathrm{e}}(\nabla d_\epsilon)} \Big(T^{\mathrm{i}}(\nabla d_\epsilon) + T^{\mathrm{e}}(\nabla d_\epsilon) \Big) \right). \end{aligned} \tag{3.25}$$

Notice that, from (3.18) and (3.24) it also follows

$$T^o(\nabla d_\epsilon) = \frac{1}{\alpha^{\mathrm{i}}(\nabla d_\epsilon)^2} T^{\mathrm{i}}(\nabla d_\epsilon) + \frac{1}{\alpha^{\mathrm{e}}(\nabla d_\epsilon)^2} T^{\mathrm{e}}(\nabla d_\epsilon).$$

Collecting all terms of order one in (3.13), remembering once more that U_0 and W_0 do not depend explicitly on s and t, we obtain for the order one, in the elliptic equation,

$$\begin{aligned} & \Big(\alpha^{\mathrm{i}}(\nabla d_\epsilon) + \alpha^{\mathrm{e}}(\nabla d_\epsilon) \Big) W_1'' - \alpha^{\mathrm{e}}(\nabla d_\epsilon) U_1'' \\ & + \underbrace{W_0' \mathrm{div} \Big(T^{\mathrm{i}}(\nabla d_\epsilon) + T^{\mathrm{e}}(\nabla d_\epsilon) \Big)}_{:=A} + 2 \langle \nabla W_0', T^{\mathrm{i}}(\nabla d_\epsilon) + T^{\mathrm{e}}(\nabla d_\epsilon) \rangle \underbrace{- U_0' \mathrm{div} T^{\mathrm{e}}(\nabla d_\epsilon)}_{:=B} = 0. \end{aligned} \tag{3.26}$$

We want to isolate a term involving $\mathrm{div} T^o(\nabla d_\epsilon)$ from $A + B$, by employing (3.25).
From (3.20) and the obvious relation

$$\begin{aligned} & \mathrm{div} \left(\frac{1}{\alpha^{\mathrm{i}}(\nabla d_\epsilon) + \alpha^{\mathrm{e}}(\nabla d_\epsilon)} (T^{\mathrm{i}}(\nabla d_\epsilon) + T^{\mathrm{e}}(\nabla d_\epsilon)) \right) \\ =& \langle T^{\mathrm{i}}(\nabla d_\epsilon) + T^{\mathrm{e}}(\nabla d_\epsilon), \nabla \frac{1}{\alpha^{\mathrm{i}}(\nabla d_\epsilon) + \alpha^{\mathrm{e}}(\nabla d_\epsilon)} \rangle + \frac{1}{\alpha^{\mathrm{i}}(\nabla d_\epsilon) + \alpha^{\mathrm{e}}(\nabla d_\epsilon)} \mathrm{div} (T^{\mathrm{i}}(\nabla d_\epsilon) + T^{\mathrm{e}}(\nabla d_\epsilon)), \end{aligned}$$

we deduce, using the identity $\alpha^{\mathrm{i}}(\nabla d_\epsilon) + \alpha^{\mathrm{e}}(\nabla d_\epsilon) = \alpha^{\mathrm{i}}(\nabla d_\epsilon) \alpha^{\mathrm{e}}(\nabla d_\epsilon)$ (see (3.18)),

$$\begin{aligned} A =& \frac{U_0'}{\alpha^{\mathrm{i}}(\nabla d_\epsilon)} \mathrm{div} \Big(T^{\mathrm{i}}(\nabla d_\epsilon) + T^{\mathrm{e}}(\nabla d_\epsilon) \Big) \\ =& U_0' \, \frac{\alpha^{\mathrm{i}}(\nabla d_\epsilon) + \alpha^{\mathrm{e}}(\nabla d_\epsilon)}{\alpha^{\mathrm{i}}(\nabla d_\epsilon)} \mathrm{div} \left(\frac{1}{\alpha^{\mathrm{i}}(\nabla d_\epsilon) + \alpha^{\mathrm{e}}(\nabla d_\epsilon)} (T^{\mathrm{i}}(\nabla d_\epsilon) + T^{\mathrm{e}}(\nabla d_\epsilon)) \right) \\ & - U_0' \frac{\alpha^{\mathrm{i}}(\nabla d_\epsilon) + \alpha^{\mathrm{e}}(\nabla d_\epsilon)}{\alpha^{\mathrm{i}}(\nabla d_\epsilon)} \langle T^{\mathrm{i}}(\nabla d_\epsilon) + T^{\mathrm{e}}(\nabla d_\epsilon), \nabla \frac{1}{\alpha^{\mathrm{i}}(\nabla d_\epsilon) + \alpha^{\mathrm{e}}(\nabla d_\epsilon)} \rangle \\ =& U_0' \, \alpha^{\mathrm{e}}(\nabla d_\epsilon) \Bigg[\mathrm{div} \left(\frac{1}{\alpha^{\mathrm{i}}(\nabla d_\epsilon) + \alpha^{\mathrm{e}}(\nabla d_\epsilon)} (T^{\mathrm{i}}(\nabla d_\epsilon) + T^{\mathrm{e}}(\nabla d_\epsilon)) \right) \\ & \qquad - \langle T^{\mathrm{i}}(\nabla d_\epsilon) + T^{\mathrm{e}}(\nabla d_\epsilon), \nabla \frac{1}{\alpha^{\mathrm{i}}(\nabla d_\epsilon) + \alpha^{\mathrm{e}}(\nabla d_\epsilon)} \rangle \Bigg]. \end{aligned}$$

We also rewrite B as

$$B = U_0' \alpha^{\mathrm{e}}(\nabla d_\epsilon) \Bigg[- \operatorname{div} \left(\frac{1}{\alpha^{\mathrm{e}}(\nabla d_\epsilon)} T^{\mathrm{e}}(\nabla d_\epsilon) \right) + \langle T^{\mathrm{e}}(\nabla d_\epsilon), \nabla \frac{1}{\alpha^{\mathrm{e}}(\nabla d_\epsilon)} \rangle \Bigg].$$

We then find

$$\begin{aligned} & A + B \\ =& U_0' \alpha^{\mathrm{e}}(\nabla d_\epsilon) \Bigg[\operatorname{div} \left(\frac{1}{\alpha^{\mathrm{i}}(\nabla d_\epsilon) + \alpha^{\mathrm{e}}(\nabla d_\epsilon)} (T^{\mathrm{i}}(\nabla d_\epsilon) + T^{\mathrm{e}}(\nabla d_\epsilon)) \right) - \operatorname{div} \left(\frac{1}{\alpha^{\mathrm{e}}(\nabla d_\epsilon)} T^{\mathrm{e}}(\nabla d_\epsilon) \right) \\ & - \langle T^{\mathrm{i}}(\nabla d_\epsilon) + T^{\mathrm{e}}(\nabla d_\epsilon), \nabla \frac{1}{\alpha^{\mathrm{i}}(\nabla d_\epsilon) + \alpha^{\mathrm{e}}(\nabla d_\epsilon)} \rangle + \langle T^{\mathrm{e}}(\nabla d_\epsilon), \nabla \frac{1}{\alpha^{\mathrm{e}}(\nabla d_\epsilon)} \rangle \Bigg], \end{aligned} \tag{3.27}$$

from which we can extract the term $\operatorname{div} T^o(\nabla d_\epsilon)$ via relation (3.25), thus obtaining

$$\begin{aligned} A + B =& U_0' \alpha^{\mathrm{e}}(\nabla d_\epsilon) \Bigg[- \operatorname{div} T^o(\nabla d_\epsilon) + \operatorname{div} \frac{1}{\alpha^{\mathrm{i}}(\nabla d_\epsilon)} T^{\mathrm{i}}(\nabla d_\epsilon) \\ & - \langle T^{\mathrm{i}}(\nabla d_\epsilon) + T^{\mathrm{e}}(\nabla d_\epsilon), \nabla \frac{1}{\alpha^{\mathrm{i}}(\nabla d_\epsilon) + \alpha^{\mathrm{e}}(\nabla d_\epsilon)} \rangle + \langle T^{\mathrm{e}}(\nabla d_\epsilon), \nabla \frac{1}{\alpha^{\mathrm{e}}(\nabla d_\epsilon)} \rangle \Bigg]. \end{aligned} \tag{3.28}$$

Inserting this results into (3.26) and using once more (3.18), we get

$$\begin{aligned} & \alpha^{\mathrm{i}}(\nabla d_\epsilon) \alpha^{\mathrm{e}}(\nabla d_\epsilon) W_1'' = (\alpha^{\mathrm{i}}(\nabla d_\epsilon) + \alpha^{\mathrm{e}}(\nabla d_\epsilon)) W_1'' \\ =& \alpha^{\mathrm{e}}(\nabla d_\epsilon) U_1'' + U_0' \alpha^{\mathrm{e}}(\nabla d_\epsilon) \Bigg[\operatorname{div} T^o(\nabla d_\epsilon) - \operatorname{div} \frac{1}{\alpha^{\mathrm{i}}(\nabla d_\epsilon)} T^{\mathrm{i}}(\nabla d_\epsilon) \\ & + \langle T^{\mathrm{i}}(\nabla d_\epsilon) + T^{\mathrm{e}}(\nabla d_\epsilon), \nabla \frac{1}{\alpha^{\mathrm{i}}(\nabla d_\epsilon) + \alpha^{\mathrm{e}}(\nabla d_\epsilon)} \rangle - \langle T^{\mathrm{e}}(\nabla d_\epsilon), \nabla \frac{1}{\alpha^{\mathrm{e}}(\nabla d_\epsilon)} \rangle \Bigg] \\ & - 2 \langle \nabla W_0', T^{\mathrm{i}}(\nabla d_\epsilon) + T^{\mathrm{e}}(\nabla d_\epsilon) \rangle, \end{aligned} \tag{3.29}$$

that we rewrite more conveniently as

$$\begin{aligned} & \alpha^{\mathrm{i}}(\nabla d_\epsilon) W_1'' \\ =& U_1'' + U_0' \Bigg[\operatorname{div} T^o(\nabla d_\epsilon) - \operatorname{div} \frac{1}{\alpha^{\mathrm{i}}(\nabla d_\epsilon)} T^{\mathrm{i}}(\nabla d_\epsilon) \\ & + \langle T^{\mathrm{i}}(\nabla d_\epsilon) + T^{\mathrm{e}}(\nabla d_\epsilon), \nabla \frac{1}{\alpha^{\mathrm{i}}(\nabla d_\epsilon) + \alpha^{\mathrm{e}}(\nabla d_\epsilon)} \rangle - \langle T^{\mathrm{e}}(\nabla d_\epsilon), \nabla \frac{1}{\alpha^{\mathrm{e}}(\nabla d_\epsilon)} \rangle \Bigg] \\ & - \frac{2}{\alpha^{\mathrm{e}}(\nabla d_\epsilon)} \langle \nabla W_0', T^{\mathrm{i}}(\nabla d_\epsilon) + T^{\mathrm{e}}(\nabla d_\epsilon) \rangle. \end{aligned} \tag{3.30}$$

We now insert this result into the expansion of the parabolic equation. Collecting all terms

of order one in (3.12), using (3.30) and (3.20), we obtain

$$
\begin{aligned}
&-U_1'' + U_1 f'(U_0) = \\
&U_0'\Bigg[- V_0 + \mathrm{div} T^o(\nabla d_\epsilon) - \mathrm{div}\frac{1}{\alpha^{\mathrm{i}}(\nabla d_\epsilon)} T^{\mathrm{i}}(\nabla d_\epsilon) \\
&\qquad + \langle T^{\mathrm{i}}(\nabla d_\epsilon) + T^{\mathrm{e}}(\nabla d_\epsilon), \nabla \frac{1}{\alpha^{\mathrm{i}}(\nabla d_\epsilon) + \alpha^{\mathrm{e}}(\nabla d_\epsilon)} \rangle - \langle T^{\mathrm{e}}(\nabla d_\epsilon), \nabla \frac{1}{\alpha^{\mathrm{e}}(\nabla d_\epsilon)} \rangle \Bigg] \\
&\underbrace{+ W_0' \mathrm{div} T^{\mathrm{i}}(\nabla d_\epsilon) + 2\langle \nabla W_0', T^{\mathrm{i}}(\nabla d_\epsilon)\rangle - \frac{2}{\alpha^{\mathrm{e}}(\nabla d_\epsilon)} \langle \nabla W_0', T^{\mathrm{i}}(\nabla d_\epsilon) + T^{\mathrm{e}}(\nabla d_\epsilon)\rangle}_{=:C} .
\end{aligned}
$$

We have, using (3.20),

$$
\begin{aligned}
C =& U_0' \frac{1}{\alpha^{\mathrm{i}}(\nabla d_\epsilon)} \mathrm{div} T^{\mathrm{i}}(\nabla d_\epsilon) + 2U_0' \langle T^{\mathrm{i}}(\nabla d_\epsilon), \nabla \frac{1}{\alpha^{\mathrm{i}}(\nabla d_\epsilon)} \rangle \\
&- \frac{2}{\alpha^{\mathrm{e}}(\nabla d_\epsilon)} U_0' \langle T^{\mathrm{i}}(\nabla d_\epsilon) + T^{\mathrm{e}}(\nabla d_\epsilon), \nabla \frac{1}{\alpha^{\mathrm{i}}(\nabla d_\epsilon)} \rangle .
\end{aligned}
$$

Hence

$$
\begin{aligned}
&-U_1'' + U_1 f'(U_0) = U_0' \Bigg[- V_0 + \mathrm{div} T^o(\nabla d_\epsilon) \\
&\underbrace{-\mathrm{div}\frac{1}{\alpha^{\mathrm{i}}(\nabla d_\epsilon)} T^{\mathrm{i}}(\nabla d_\epsilon) + \frac{1}{\alpha^{\mathrm{i}}(\nabla d_\epsilon)} \mathrm{div} T^{\mathrm{i}}(\nabla d_\epsilon)}_{=:D} \\
&+ \langle T^{\mathrm{i}}(\nabla d_\epsilon) + T^{\mathrm{e}}(\nabla d_\epsilon), \nabla \frac{1}{\alpha^{\mathrm{i}}(\nabla d_\epsilon) + \alpha^{\mathrm{e}}(\nabla d_\epsilon)} \rangle - \langle T^{\mathrm{e}}(\nabla d_\epsilon), \nabla \frac{1}{\alpha^{\mathrm{e}}(\nabla d_\epsilon)} \rangle \\
&+ 2\langle T^{\mathrm{i}}(\nabla d_\epsilon), \nabla \frac{1}{\alpha^{\mathrm{i}}(\nabla d_\epsilon)} \rangle - \frac{2}{\alpha^{\mathrm{e}}(\nabla d_\epsilon)} \langle T^{\mathrm{i}}(\nabla d_\epsilon) + T^{\mathrm{e}}(\nabla d_\epsilon), \nabla \frac{1}{\alpha^{\mathrm{i}}(\nabla d_\epsilon)} \rangle \Bigg] .
\end{aligned}
$$

Since $D = -\langle T^{\mathrm{i}}(\nabla d_\epsilon), \nabla \frac{1}{\alpha^{\mathrm{i}}(\nabla d_\epsilon)} \rangle$, we have

$$
-U_1'' + U_1 f'(U_0) = U_0' \Bigg(- V_0 + \mathrm{div} T^o(\nabla d_\epsilon) + E \Bigg)
$$

where

$$
\begin{aligned}
E =& \langle T^{\mathrm{i}}(\nabla d_\epsilon), \nabla \frac{1}{\alpha^{\mathrm{i}}(\nabla d_\epsilon)} \rangle - \langle T^{\mathrm{e}}(\nabla d_\epsilon), \nabla \frac{1}{\alpha^{\mathrm{e}}(\nabla d_\epsilon)} \rangle \\
&+ \langle T^{\mathrm{i}}(\nabla d_\epsilon) + T^{\mathrm{e}}(\nabla d_\epsilon), \nabla \frac{1}{\alpha^{\mathrm{i}}(\nabla d_\epsilon) + \alpha^{\mathrm{e}}(\nabla d_\epsilon)} \rangle - \frac{2}{\alpha^{\mathrm{e}}(\nabla d_\epsilon)} \langle T^{\mathrm{i}}(\nabla d_\epsilon) + T^{\mathrm{e}}(\nabla d_\epsilon), \nabla \frac{1}{\alpha^{\mathrm{i}}(\nabla d_\epsilon)} \rangle .
\end{aligned}
$$

Observe that, using (3.23),

$$
\begin{aligned}
&\nabla \frac{1}{\alpha^{\mathrm{i}}(d_\epsilon) + \alpha^{\mathrm{e}}(d_\epsilon)} = \nabla \frac{1}{\alpha^{\mathrm{i}}(\nabla d_\epsilon)\alpha^{\mathrm{e}}(\nabla d_\epsilon)} = \frac{1}{\alpha^{\mathrm{i}}(\nabla d_\epsilon)} \nabla \frac{1}{\alpha^{\mathrm{e}}(\nabla d_\epsilon)} + \frac{1}{\alpha^{\mathrm{e}}(\nabla d_\epsilon)} \nabla \frac{1}{\alpha^{\mathrm{i}}(\nabla d_\epsilon)} \\
=& - \frac{1}{\alpha^{\mathrm{i}}(\nabla d_\epsilon)} \nabla \frac{1}{\alpha^{\mathrm{i}}(\nabla d_\epsilon)} + \frac{1}{\alpha^{\mathrm{e}}(\nabla d_\epsilon)} \nabla \frac{1}{\alpha^{\mathrm{i}}(\nabla d_\epsilon)}
\end{aligned}
$$

Hence, expressing $\nabla\frac{1}{\alpha^{\mathrm{e}}}$ using $\nabla\frac{1}{\alpha^{\mathrm{i}}}$ in E, we get

$$E = \left(1 - \frac{1}{\alpha^{\mathrm{i}}(\nabla d_\epsilon)} - \frac{1}{\alpha^{\mathrm{e}}(\nabla d_\epsilon)}\right)\langle T^{\mathrm{i}}(\nabla d_\epsilon) + T^{\mathrm{e}}(\nabla d_\epsilon), \nabla\frac{1}{\alpha^{\mathrm{i}}(\nabla d_\epsilon)}\rangle = 0,$$

since $\frac{1}{\alpha^{\mathrm{i}}(\nabla d_\epsilon)} + \frac{1}{\alpha^{\mathrm{e}}(\nabla d_\epsilon)} = 1$. We conclude, using the expansion of $\mathrm{div}T^o(\nabla d_\epsilon)$ in terms of the φ-anisotropic mean curvature κ_ϵ,

$$-U_1'' + f'(U_0)U_1 = U_0'\Big[V_0 - \kappa_0\Big].$$

From (3.8) and the Fredholm alternative (see for instance [9]) we end up with the remarkable result

$$V_0 = -\kappa_0 \tag{3.31}$$

so that $U_1 = 0$.
We are now in a position to recover the first term w_0 of the outer expansion of w_ϵ by adding to (3.4) a jump condition for w_0 and for $\langle n_0^\varphi, \nabla w_0\rangle$ across the interface[16] $\Sigma_0(t)$. For this derivation it is convenient to write W_1'' from (3.30) in an alternative form: we have

$$W_1'' = U_0'\left\{\mathrm{div}\left[\frac{1}{\alpha^{\mathrm{i}}}T^o(\nabla d_\epsilon) - \frac{1}{(\alpha^{\mathrm{i}})^2}T^{\mathrm{i}}(\nabla d_\epsilon)\right] - \nabla\frac{1}{\alpha^{\mathrm{i}}}\cdot T^o(\nabla d_\epsilon)\right\},$$

where we used twice $\frac{1}{\alpha^{\mathrm{i}}}\mathrm{div}(\star) = \mathrm{div}(\frac{1}{\alpha^{\mathrm{i}}}\star) - \nabla\frac{1}{\alpha^{\mathrm{i}}}\cdot\star$; definition (3.20); $\nabla\frac{1}{\alpha^{\mathrm{i}}+\alpha^{\mathrm{e}}} = \nabla\frac{1}{\alpha^{\mathrm{i}}\alpha^{\mathrm{e}}} = \frac{1}{\alpha^{\mathrm{i}}}\nabla\frac{1}{\alpha^{\mathrm{e}}} + \frac{1}{\alpha^{\mathrm{e}}}\nabla\frac{1}{\alpha^{\mathrm{i}}}$; $\nabla\frac{1}{\alpha^{\mathrm{e}}} = -\nabla\frac{1}{\alpha^{\mathrm{i}}}$ and $\frac{1}{\alpha^{\mathrm{e}}} = 1 - \frac{1}{\alpha^{\mathrm{i}}}$.
By recalling $T^o(\nabla d_\epsilon) = Q(\nabla d_\epsilon)\nabla d_\epsilon = \frac{1}{(\alpha^{\mathrm{i}})^2}T^{\mathrm{i}}(\nabla d_\epsilon) + \frac{1}{(\alpha^{\mathrm{e}})^2}T^{\mathrm{e}}(\nabla d_\epsilon)$, see (2.3)[17], expanding the first term in the divergence and collecting terms involving T^{i} (resp. T^{e}), we finally arrive at

$$W_1'' = U_0'\left\{\mathrm{div}\frac{1}{\alpha^M}\left[\frac{1}{\alpha^{\mathrm{e}}}T^{\mathrm{e}}(\nabla d_\epsilon) - \frac{1}{\alpha^{\mathrm{i}}}T^{\mathrm{i}}(\nabla d_\epsilon)\right] - \nabla\frac{1}{\alpha^{\mathrm{i}}}\cdot T^o(\nabla d_\epsilon)\right\}. \tag{3.32}$$

From (3.20) we get

$$[\![w_0]\!] = \frac{2}{\alpha^{\mathrm{i}}(\nabla d_\epsilon)}. \tag{3.33}$$

Using (3.17), (3.32), and again (3.20), recalling that $n^\varphi = -T^o(\nabla d_\epsilon)$, we end up with

$$-[\![\langle n_0^\varphi, \nabla w_0\rangle]\!] = 2\mathrm{div}\left[\frac{1}{\alpha^M}\left(\frac{1}{\alpha^{\mathrm{e}}}T^{\mathrm{e}}(\nabla d_\epsilon) - \frac{1}{\alpha^{\mathrm{i}}}T^{\mathrm{i}}(\nabla d_\epsilon)\right)\right]. \tag{3.34}$$

The two jump conditions on w_0 across $\Sigma_0(t)$, together with equation (3.4) and appropriate boundary conditions at $\partial\Omega$, allow to obtain a unique solution w_0.
Note that the jump in the *conormal* derivative $[\![\langle n_0^\varphi, \nabla w_0\rangle]\!]$ vanishes in the special case $\alpha^{\mathrm{e}} = \lambda\alpha^{\mathrm{i}}$, and hence $T^{\mathrm{e}} = \lambda T^{\mathrm{i}}$ (equal anisotropic ratio).

[16] We will assume that $\Sigma_\epsilon(t)$ can be expanded in ϵ, and written as a graph over an hypersurface at $\epsilon = 0$ along the direction n_0^φ. We denote by $\Sigma_0(t)$ such an hypersurface.

[17] Remember that from the definition of d_ϵ we have $\alpha^{\mathrm{i}} + \alpha^{\mathrm{e}} = \alpha^{\mathrm{i}}\alpha^{\mathrm{e}}$.

4 On the nonconvexity of the combined anisotropy

Recalling (1.8), the Frank diagram F_Φ of Φ is the set

$$F_\Phi = \{\xi^\star \in \mathbb{R}^d : \alpha^{\mathrm{i}}(\xi^\star) + \alpha^{\mathrm{e}}(\xi^\star) \geq \alpha^{\mathrm{i}}(\xi^\star)\alpha^{\mathrm{e}}(\xi^\star)\} = \{\xi^\star \in \mathbb{R}^d : J(\xi^\star) \leq 0\} \tag{4.1}$$

where $J(\xi^\star) := \alpha^{\mathrm{i}}(\xi^\star)\alpha^{\mathrm{e}}(\xi^\star) - \alpha^{\mathrm{i}}(\xi^\star) - \alpha^{\mathrm{e}}(\xi^\star)$. The inequality above becomes an equality only if $\xi^\star$ is the origin or if it belongs to the boundary of the Frank diagram.
In the *linear* case, function J is a polinomial of degree four in the components of $\xi^\star$. From the equivalence of all norms in finite dimension it follows that both α^{i} and α^{e} can be bounded from below and above by $m|\xi^\star|^2$ and $M|\xi^\star|^2$ for suitable constants $0 < m < M$ independent of $\xi^\star$, so that

$$\alpha^{\mathrm{i}}\alpha^{\mathrm{e}} \leq M^2|\xi^\star|^4, \qquad \alpha^{\mathrm{i}} + \alpha^{\mathrm{e}} \geq 2m|\xi^\star|^2$$

and $J(\xi^\star) < 0$ for $|\xi^\star|$ sufficiently small and nonzero. Similarly we see that $J(\xi^\star) > 0$ for $|\xi^\star|$ sufficiently large. For a given $\bar{\xi}$, function $p(t) = J(t\xi^\star)$ is a polinomial of degree four with a double zero at the origin (because $p(0) = 0$ and is nonpositive near 0) and has two more zeros simmetrically placed with respect to the origin since p is positive at $\pm\infty$. Since we have collected all the zeros of p we conclude that the set $p(t) \leq 0$ is a segment centered at the origin, and in the end F_Φ is symmetric and star-shaped about the origin. However, it is not in general convex.
We shall now restrict to the case of *inverted anisotropic ratio* and consider the special case where the matrices M^{i} and M^{e} are given by

$$M^{\mathrm{i}} := \begin{bmatrix} 1 & 0 \\ 0 & \rho \end{bmatrix}, \qquad M^{\mathrm{e}} := \begin{bmatrix} \rho & 0 \\ 0 & 1 \end{bmatrix}, \qquad \rho > 0. \tag{4.2}$$

The results of this section will also be valid whenever the two matrices are transformed in the form above after scaling and rotation.

4.1 Identifying the nonconvex regime for inverted anisotropic ratio

If $\xi^\star = (\cos\theta, \sin\theta)$ we can express $\varphi^o(\xi^\star)$ in terms of θ as $\varphi^o(\xi^\star) = \gamma(\theta)$ with

$$\gamma = \gamma(\theta) = \sqrt{\frac{\alpha^{\mathrm{i}}\alpha^{\mathrm{e}}}{\alpha^{\mathrm{i}} + \alpha^{\mathrm{e}}}}, \qquad \alpha^{\mathrm{i}} = \cos^2\theta + \rho\sin^2\theta, \qquad \alpha^{\mathrm{e}} = \sin^2\theta + \rho\cos^2\theta \tag{4.3}$$

now

$$\begin{aligned} 8\alpha^{\mathrm{i}}\alpha^{\mathrm{e}} =& 8\cos^2\theta\sin^2\theta + 8\rho\cos^4\theta + 8\rho\sin^4\theta + 8\rho^2\cos^2\theta\sin^2\theta \\ =& 2(1+\rho^2)\sin^2 2\theta + 4\rho(1+\cos^2 2\theta) \\ =& 4\rho + (1+\rho^2)(1-\cos 4\theta) + 2\rho(1+\cos 4\theta) \\ =& \rho^2 + 6\rho + 1 - (\rho-1)^2\cos 4\theta \end{aligned}$$

and

$$\alpha^{\mathrm{i}} + \alpha^{\mathrm{e}} = \rho + 1$$

whence

$$8(\rho+1)\gamma^2 = \rho^2 + 6\rho + 1 - (\rho-1)^2\cos 4\theta \tag{4.4}$$

Differentiating with respect to θ we get:

$$16(\rho+1)\gamma\gamma_\theta = 4(\rho-1)^2 \sin 4\theta \tag{4.5}$$

Differentiating again we get:

$$16(\rho+1)(\gamma\gamma_{\theta\theta} + \gamma_\theta^2) = 16(\rho-1)^2 \cos 4\theta$$

which allows to express the second derivative $\gamma_{\theta\theta}$ as

$$\gamma_{\theta\theta} = \frac{(\rho-1)^2 \cos 4\theta - (\rho+1)\gamma_\theta^2}{(\rho+1)\gamma} \tag{4.6}$$

It is well known that convexity of the Frank diagram of an anisotropy expressed in polar form as above is equivalent to $\gamma + \gamma_{\theta\theta} \geq 0$, or, equivalently, to $8(\rho+1)\gamma^2 + 8(\rho+1)\gamma\gamma_{\theta\theta} \geq 0$, since γ is positive for all θ. By combining (4.4) and (4.6) we then get

$$8(\rho+1)\gamma(\gamma+\gamma_{\theta\theta}) = \rho^2 + 6\rho + 1 + 7(\rho-1)^2\cos 4\theta - 8(\rho+1)\gamma_\theta^2$$

Equation (4.5) and (4.4) allows to compute $8(\rho+1)\gamma_\theta^2$ as

$$8(\rho+1)\gamma_\theta^2 = \frac{(\rho-1)^4 \sin^2 4\theta}{2(\rho+1)\gamma^2} = \frac{4(\rho-1)^4 - 4(\rho-1)^4\cos^2 4\theta}{\rho^2+6\rho+1-(\rho-1)^2\cos 4\theta}$$

so that by writing Θ in place of $(\rho-1)^2\cos 4\theta$ we arrive at

$$\begin{aligned} 8(\rho+1)\gamma(\gamma+\gamma_{\theta\theta}) =& \rho^2+6\rho+1+7\Theta - \frac{4(\rho-1)^4 - 4\Theta^2}{\rho^2+6\rho+1-\Theta} \\ =& \frac{-3\Theta^2 + 6(\rho^2+6\rho+1)\Theta + (3\rho^2+2\rho+3)(-\rho^2+10\rho-1)}{\rho^2+6\rho+1-\Theta} \end{aligned}$$

By (4.4) the denominator is actually $8(\rho+1)\gamma^2$ and is always strictly positive, hence it suffices to study the sign of the numerator N. Recalling the definition of Θ above N can be written as

$$N = -3(\rho-1)^4\cos^2 4\theta + 6(\rho^2+6\rho+1)(\rho-1)^2\cos 4\theta - (3\rho^2+2\rho+3)(\rho^2-10\rho+1)$$

which is a second degree polynomial in $\cos 4\theta$ with roots

$$c_\pm = \frac{\rho^2+6\rho+1 \pm 8(\rho+1)\sqrt{\frac{\rho}{3}}}{(\rho-1)^2}.$$

They are invariant under the change $\rho \to \frac{1}{\rho}$ which suggests the change of variables $\sigma = \frac{1}{\sqrt{3}}\left(\sqrt{\rho} + \frac{1}{\sqrt{\rho}}\right)$ (note that $\sqrt{3}\sigma > 2$ for all $\rho > 0$). We arrive at

$$c_\pm = \frac{3\sigma^2 + 4 \pm 8\sigma}{3\sigma^2 - 4}.$$

The larger root c_+ is always larger than 1, so that the only possible zeros of the numerator are solutions of

$$\cos 4\theta = \frac{(3\sigma-2)(\sigma-2)}{3\sigma^2-4}.$$

The right-hand side is strictly increasing for $\sigma > \frac{2}{\sqrt{3}}$, goes to $-\infty$ as $\sigma \to \frac{2}{\sqrt{3}}$ from the right and goes to 1 as $\sigma \to +\infty$. It evaluates to -1 for $\sigma = \frac{4}{3}$, which corresponds to $\rho = 3$ and $\rho = \frac{1}{3}$. We have thus proved the following

Theorem 4.1. *The unit ball $\{\varphi^o \leq 1\}$ is convex if and only if $\frac{1}{3} \leq \rho \leq 3$. It is strictly convex in the open interval $\frac{1}{3} < \rho < 3$. It is convex for $\rho = 3$ or $\rho = \frac{1}{3}$ with zero curvature at the intersections with $\xi_2^\star = \pm\xi_1^\star$. It is not convex for $\rho > 3$ and $0 < \rho < \frac{1}{3}$. In this latter case, the values of θ where ∂F_Φ is concave are those that satisfy*

$$\cos 4\theta < \frac{(3\sigma-2)(\sigma-2)}{3\sigma^2-4} = \frac{\rho^2+6\rho+1-8(\rho+1)\sqrt{\frac{\rho}{3}}}{(\rho-1)^2} \tag{4.7}$$

4.2 Computing the bitangent for $\rho > 3$

With the definition (4.2), setting $\xi^\star = (x, y)$, we have:

$$\alpha^{\mathrm{i}} = x^2 + \rho y^2, \qquad \alpha^{\mathrm{e}} = \rho x^2 + y^2 \tag{4.8}$$

So that function J in $F_\Phi = \{J(\xi^\star) \leq 0\}$ can be written as

$$J(x, y) = (x^2 + \rho y^2)(\rho x^2 + y^2) - (1+\rho)(x^2+y^2). \tag{4.9}$$

We can take advantage of the symmetry of the algebraic curve defined by $J(x, y) = 0$ and look for a bitangent line of the form $x + y = h$ for some $h > 0$. We get the intersections of this line with the algebraic curve by substituting $y = h - x$ into (4.9) which gives a polynomial of degree four $p_4(x)$ in the indeterminate x with coefficients depending on ρ and h. We seek a value for h such that this polynomial is of the form $c(x-a)^2(x-b)^2$ for some $a, b \in \mathbb{R}$, i.e. it has two double zeroes, corresponding to a bitangential position of the line.
Carrying out the formal computations with `wxmaxima` we end up with

$$h = \sqrt{\frac{\rho+1}{\rho-1}}$$

which we can substitute in p_4 and solve the resulting fourth degree equation (again with `wxmaxima`) to get the x coordinate (and then the y coordinate) of one of the two contact points:

$$B_1 = \frac{1}{2}\left[\sqrt{\frac{\rho+1}{\rho-1}} + \sqrt{\frac{\rho-3}{\rho-1}}, \sqrt{\frac{\rho+1}{\rho-1}} - \sqrt{\frac{\rho-3}{\rho-1}}\right], \tag{4.10}$$

the other can be obtained by exchanging the two coordinates. Note that $|B_1| = 1$. This result has been used to produce some of the figures of Section 6.

4.3 Computing the dual norm in the convex regime

If $\frac{1}{3} \leq \rho \leq 3$ we have convexity of $\Phi = \varphi^o$ so that we have a well-defined dual norm φ given by

$$\varphi(\xi) = \sup_{\xi^\star \neq 0} \frac{\langle \xi^\star, \xi \rangle}{\varphi^o(\xi^\star)} = \max_\theta \frac{\xi_1 \cos\theta + \xi_2 \sin\theta}{\gamma(\theta)}$$

In particular, for $\xi = (\cos\eta, \sin\eta)$ we have

$$\hat{\gamma}(\alpha) = \varphi((\cos\alpha, \sin\alpha)) = \max_\theta \frac{\cos(\alpha - \theta)}{\gamma(\theta)} = \frac{\cos(\alpha - \overline{\theta})}{\gamma(\overline{\theta})}$$

Finding the maximum point $\overline{\theta}$ amounts to solve the following algebraic equation of degree 5 for x in terms of y, after substituting (4.4) where $x = \tan\overline{\theta}$, $y = \tan\alpha$

$$p(x) = x^5 - \sigma y x^4 + 2x^3 - 2yx^2 + \sigma x - y = 0$$

with $\sigma = \rho + \frac{1}{\rho} - 1$, so that $1 \leq \sigma \leq \frac{7}{3}$
A graphic plot of p and p'' as a function of x for various values of σ and y suggests that if $\sigma \leq 2$ the polynomial is convex between its only root in the interval $[0, 1]$ and the value $y \in [0, 1]$ which implies we can employ the Newton method for solving $p(x) = 0$ with y as a starting value. This procedure has been used to obtain the initial datum for the first simulation of Section 6, see Figure 3.

5 Discretization

We employ standard piecewise linear finite elements in space and a forward difference scheme in time. $\Omega \in \mathbb{R}^2$ is assumed to be a two-dimensional polygonal domain. Problem (1.1) will be approximated in the special *linear* case described in Section 1.1, see (1.9).
The weak formulation of the parabolic/elliptic formulation (compare (3.2)) reads as

$$\begin{cases} \left((M^{\mathrm{i}} + M^{\mathrm{e}})\nabla w_\epsilon, v\right)_{L^2(\Omega)} - (M^{\mathrm{e}}\nabla u_\epsilon, v)_{L^2(\Omega)} = 0 & \forall v \in H^1_0(\Omega), \\ \epsilon^2 \left(\partial_t u_\epsilon, v\right)_{L^2(\Omega)} - \epsilon^2 \left(M^{\mathrm{i}}\nabla w_\epsilon, v\right)_{L^2(\Omega)} + (f(u_\epsilon), v))_{L^2(\Omega)} = 0 & \forall v \in H^1_0(\Omega), \end{cases} \tag{5.1}$$

with[18] $u_\epsilon(\cdot, t) \in H^1_u(\Omega) := \{u \in H^1(\Omega) : \mathrm{Tr}(u) = 1\}$, $w_\epsilon(\cdot, t) \in H^1_w(\Omega) := \{u \in H^1(\Omega) : \mathrm{Tr}(u) = g_w\}$, for a given boundary datum g_w.
For a given $h > 0$ (space discretization parameter) we construct a subdivision $T_h = \{K : K \in T_h\}$ of $\overline{\Omega}$ with triangles K with $\mathrm{diam}(K) \leq h$ such that $\overline{\Omega} = \cup_{K \in T_h} K$ and satisfying the usual compatibility conditions of finite element subdivisions [13].
The finite element spaces V^h and V^h_0 and the affine spaces V^h_u, V^h_w are defined by

$$\begin{aligned} V^h &:= \{v \in C^0(\overline{\Omega}) : v_{|K} \in \mathbb{P}^1(K)\ \forall K \in T_h\}, \\ V^h_0 &:= V^h \cap H^1_0(\Omega), \\ V^h_u &:= \{v \in V^h : v_{|\partial\Omega} = 1\}, \\ V^h_w &:= \{v \in V^h : v_{|\partial\Omega} = \Pi_h(g_w)\}. \end{aligned}$$

[18] We fix Dirichlet boundary conditions for the two unknown functions as $u_\epsilon = 1$ at $\partial\Omega$ (the evolving phase $u_\epsilon)\cdot, t) \approx -1$ is compactly contained in Ω) and $w_\epsilon = g_w$.

Then for a given $\tau > 0$ (time discretization parameter) and initial datum $u_h^{(0)} \in V_u^h$, the fully discrete problem consists in finding functions $w_h^{(n)} \in V_u^h$, $n = 0, \dots, N$ and $u_h^{(n)} \in V_w^h$, $n = 1, \dots, N$ (from which we can readily retrieve an approximation of u_ϵ^{i} and u_ϵ^{e}) such that

$$\begin{cases} \left((M^{\mathrm{i}} + M^{\mathrm{e}})\nabla w_h^{(n)}, \nabla v_h\right)_{L^2(\Omega)} - \left(M^{\mathrm{e}}\nabla u_h^{(n)}, \nabla v_h\right)_{L^2(\Omega)} = 0 & \forall v_h \in V_0^h, \\ \left(u_h^{(n+1)} - u_h^{(n)}, v_h\right)_{L^2(\Omega)}^h - \tau\left(M^{\mathrm{i}}\nabla w_h^{(n)}, \nabla v_h\right)_{L^2(\Omega)} + \frac{\tau}{\epsilon^2}\left(f(u_h^{(n)}), v_h\right)_{L^2(\Omega)}^h = 0 & \forall v_h \in V_0^h. \end{cases} \tag{5.2}$$

The notation $(v, w)_{L^2(\Omega)}^h = \int_\Omega \Pi_h(vw)\, dx$ indicates the use of the trapezoidal quadrature rule to approximate the exact L^2 scalar product, which leads to a diagonal mass matrix (mass lumping). Functions $u_h^{(n)}$ and $w_h^{(n)}$ represent an approximation of the exact solution $u_\epsilon^{\mathrm{i}}(\cdot, t_n) - u_\epsilon^{\mathrm{e}}(\cdot, t_n)$ and $u_\epsilon^{\mathrm{i}}(\cdot, t_n)$ at time $t_n = n\tau$, $n = 0, \dots, N$.
Let $\{x_j\}_{j=1}^J$ be the internal nodes (vertices of the triangular elements) of T_h and $\{\phi_j\}_{j=1}^J$ the corresponding nodal basis of V_0^h. Function $u_h^{(n)}$ (resp. $w_h^{(n)}$) can then be written as

$$u_h^{(n)} = \hat{u}_h + \sum_{j=1}^J \mathbf{u}_j^{(n)}\phi_j, \qquad w_h^{(n)} = \hat{w}_h + \sum_{j=1}^J \mathbf{w}_j^{(n)}\phi_j,$$

where $\mathbf{u}_j^{(n)} = u_h^{(n)}(x_j)$ (resp. $\mathbf{w}_j^{(n)} = w_h^{(n)}(x_j)$), $j = 1, \dots, J$, and $\hat{u}_h \in V_u^h$ (resp. $\hat{w}_h \in V_w^h$) is a fixed function that vanishes at all internal node and takes care of the Dirichlet boundary datum.
We can now test the two equations in (5.2) against each of the basis functions ϕ_i, $i = 1, \dots, J$ to obtain the matrix formulation

$$\begin{cases} A\mathbf{w}^{(n)} = A^{\mathrm{e}}\mathbf{u}^{(n)} + \mathbf{b}^{(n)} & n = 0, \dots, N, \\ M\mathbf{u}^{(n+1)} = M\mathbf{u}^{(n)} + \tau A^{\mathrm{i}}\mathbf{w}^{(n)} - \frac{\tau}{\epsilon^2} M f(\mathbf{u}^{(n)}) + \tau\mathbf{c} & n = 1, \dots, N, \end{cases} \tag{5.3}$$

where function f acts componentwise. With reference to the first problem (a linear system that is the discrete counterpart of the elliptic equation in (5.1)), we have two $(J \times J)$ "stiffness" matrices $A = (A_{ij})_{ij}$, $A^{\mathrm{e}} = (A_{ij}^{\mathrm{e}})_{ij}$; $\mathbf{b}^{(n)} = (\mathbf{b}_i^{(n)})_i$ is a vector in $\mathbb{R}^J$ that takes into account the Dirichlet boundary data,

$$\begin{aligned} A_{ij} &= \left((M^{\mathrm{i}} + M^{\mathrm{e}})\nabla\phi_j, \nabla\phi_i\right)_{L^2(\Omega)}, & i, j = 1, \dots, J \\ A_{ij}^{\mathrm{e}} &= \left(M^{\mathrm{e}}\nabla\phi_j, \nabla\phi_i\right)_{L^2(\Omega)}, & i, j = 1, \dots, J \\ \mathbf{b}_i^{(n)} &= \left(M^{\mathrm{e}}\nabla\hat{u}_h, \nabla\phi_i\right)_{L^2(\Omega)} - \left((M^{\mathrm{i}} + M^{\mathrm{e}})\nabla\hat{w}_h, \nabla\phi_i\right)_{L^2(\Omega)}, & i = 1, \dots, J. \end{aligned}$$

With reference to the second problem in (5.3) (the discrete counterpart of the parabolic equation in (5.1)) we have a diagonal mass matrix M, a $(J \times J)$ stiffness matrix $A^{\mathrm{i}} = (A_{ij}^{\mathrm{i}})_{ij}$ and a vector $\mathbf{c}$ defined by

$$\begin{aligned} M_{ij} &= (\phi_i, \phi_j)_{L^2(\Omega)}^h = \int_\Omega \phi_i dx\ \delta_{ij} \\ A_{ij}^{\mathrm{i}} &= \left(M^{\mathrm{i}}\nabla\phi_j, \nabla\phi_i\right)_{L^2(\Omega)} \\ \mathbf{c}_i &= \left(M^{\mathrm{i}}\nabla\hat{w}_h, \nabla\phi_i\right)_{L^2(\Omega)}. \end{aligned}$$

To obtain (5.3) we also used that $(\hat{u}_h, \phi_i)^h_{L^2(\Omega)} = 0$, for $i = 1, \ldots, J$.
The second equation in (5.3) is trivially solvable, since M is a diagonal matrix. Moreover the use of finite elements leads to a sparse matrix A^{i} with $\mathcal{O}(J)$ nonzero elements, leading to a computational cost of $\mathcal{O}(J)$ floating point operations per time step.
The first equation in (5.3) is a linear system of order J with a sparse positive definite matrix A (that the right-hand side is known from the previous time step, up to a sparse matrix-vector multiplication).
The linear system can be solved by using a preconditioned conjugate gradient method. Direct experimentation shows that a fair preconditioning can achieved using a modified incomplete Choleski factorization. This amounts to carrying out a standard Choleski LDL^t factorization exept that we force to zero elements of L corresponding to zero elements of A; moreover such neglected elements are accumulated into the diagonal matrix D. The preconditioner then takes the form $P = LDL^t$ and we need to solve at each conjugate gradient step the linear system $Pz = r$, which can be done efficiently with forward and backward substitution to solve the two triangular systems with a cost of $\mathcal{O}(J)$ due to the sparseness of L.
We solve the problem on a domain $\Omega = (-l, l) \times (-l, l)$ with initial and boundary conditions that are symmetric about the two coordinate axes. This permits to use a computational domain given by the square $(0, l) \times (0, l)$ with homogeneous Neumann boundary conditions on nodes along the coordinate axes. This particular choice of the computational domain allows the use of a structured triangulation obtained by first dividing the domain in a grid of small $h \times h$ squares with $h = l/n$ for a given n and then dividing each square in two rectangular triangles using the diagonal parallel to the bisector of the first and third quadrant.
Finally we restrict ourselves to diagonal matrices M^{i} and M^{e}. With this restriction the resulting stiffness matrices A, A^{i}, A^{e} assume a particularly simple structure with a maximum of 5 nonzero entries on each line. Moreover $A_{ij} \neq 0$ implies $|i-j| \in \{0, 1, n\}$ (recall that $J = n^2$) and similarly for A^{i} and A^{e}. Specifically, the three stiffness matrices can be regarded as block tridiagonal with $n \times n$ blocks, the blocks along the diagonal are tridiagonal $(n \times n)$ matrices, whereas the off-diagonal blocks are diagonal $(n \times n)$ matrices. Such structure allows to take advantage of a multiprocessor architecture with the important exception of the solution of the preconditioning system because of the use of forward and backward substitution, which are intrinsically sequential algorithms. Making the preconditioning system more parallelizable requires further investigation and possibly also a different choice of the preconditioning matrix.

5.1 The anisotropic Allen-Cahn equation

The matched asymptotics of Section 3 suggests that for small values of $\epsilon > 0$ the transition layer of the bidomain evolution approximates a front that evolves by anisotropic mean curvature with the combined anisotropy Φ defined in (1.8), at least when the latter anisotropy is convex (i.e. $\Phi = \varphi^o$, see Section 2.2). For a nonconvex anisotropy such a statement no longer makes sense, since anisotropic mean curvature flow becomes an ill-posed problem.
The corresponding Allen-Cahn equation (now one equation only) reads as

$$\epsilon^2 \partial_t u_\epsilon - \epsilon^2 \mathrm{div} T^o(\nabla u_\epsilon) + f(u_\epsilon) = 0, \tag{5.4}$$

where T^o is defined in (2.7). The problem is completed by adding the same initial condition (difference between u^{i}_ϵ and u^{e}_ϵ) as the one used for the bidomain problem (1.1) and Dirichlet

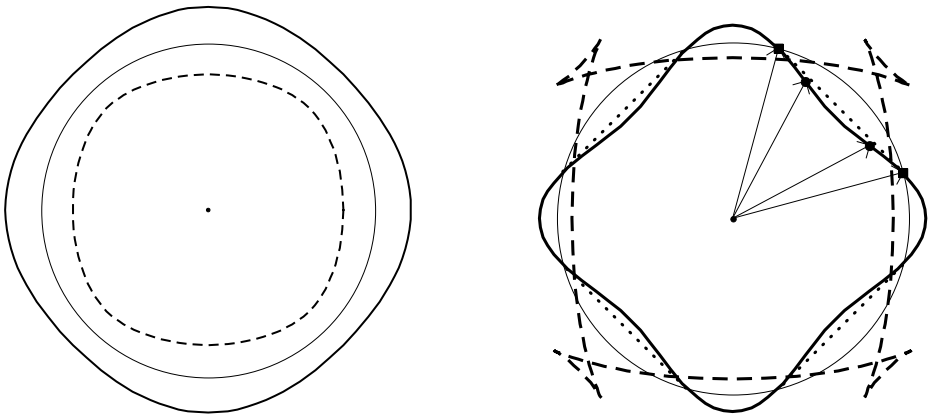

Figure 2: The Frank diagram (solid line) and Wulff shape (dashed line) for $\rho = 2$ (left) and $\rho = 5$ (right). In the nonconvex case ($\rho = 5$) the swallowtails are just artifacts that correspond to the nonconvex portions of the anisotropy.

boundary condition given by the difference between the boundary conditions enforced for (1.1). The solution of (5.4) produces an evolving transition layer that approximates the Φ-anisotropic geometric evolution (with an $\mathcal{O}(\epsilon^2)$ error) [26]. This suggests the use of the Allen-Cahn equation as a tool to provide a comparison for the bidomain solution, at least in the convex regime, i.e. for $\rho \leq 3$.
A discretization procedure for equation (5.4) is described in [33].

6 Numerical simulations

We present here two sets of numerical simulations, all for $d = 2$, corresponding to the inverted anisotropic ratio case. The matrices M^{i} and M^{e} are defined as

$$M^{\mathrm{i}} := \begin{bmatrix} 1 & 0 \\ 0 & \rho \end{bmatrix}, \qquad M^{\mathrm{e}} := \begin{bmatrix} \rho & 0 \\ 0 & 1 \end{bmatrix}. \tag{6.1}$$

6.1 Simulations with $\rho = 2$

In the first set of simulations we fix $\rho = 2$ for the inverted ratio as defined in (6.1). This leads to a convex combined anisotropy φ^o as defined in Section 2.2. Its unit ball (Frank diagram) is shown in Figure 2 left. The unit ball of the dual $\varphi = \varphi^{oo}$ of φ^o is usually referred to as the Wulff shape, and is depicted with a dashed line in Figure 2 left. Formal asymptotics suggests that the transition layer of $u_\epsilon^{\mathrm{i}} - u_\epsilon^{\mathrm{e}}$ approximates with an $\mathcal{O}(\epsilon)$ error a curve that evolves by φ-anisotropic curvature [10].
It is known that anisotropic curvature flow evolves the Wulff shape W_φ selfsimilarly, more precisely we have the following exact anisotropic curvature evolution: $\Sigma(t) = \sqrt{1-2t}\ \partial W_\varphi$. This suggests a numerical simulation of the bidomain problem on the square $(0,1) \times (0,1)$ with an initial transition region corresponding to ∂W_φ. The initial datum $u_\epsilon^{\mathrm{i}}(\cdot,0) - u_\epsilon^{\mathrm{e}}(\cdot,0)$ is thus defined by

$$\gamma\left(\frac{\varphi(x)-1}{\epsilon}\right)$$

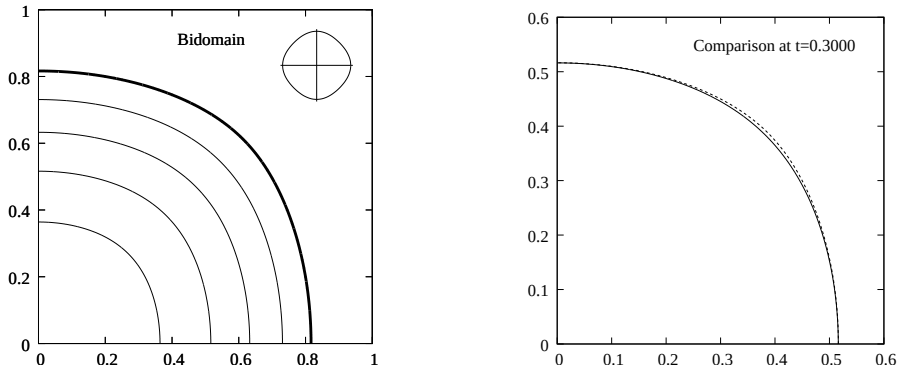

Figure 3: Left: simulation with $\rho = 2$, $\epsilon = 0.04$, $h = 0.005$ at time steps intervals of 0.1, the small plot at the top-right corner shows the Frank diagram of the combined anisotropy. The initial datum corresponds to the Wulff shape. Right: comparison at time 0.3 with the exact anisotropic mean curvature flow (dotted line).

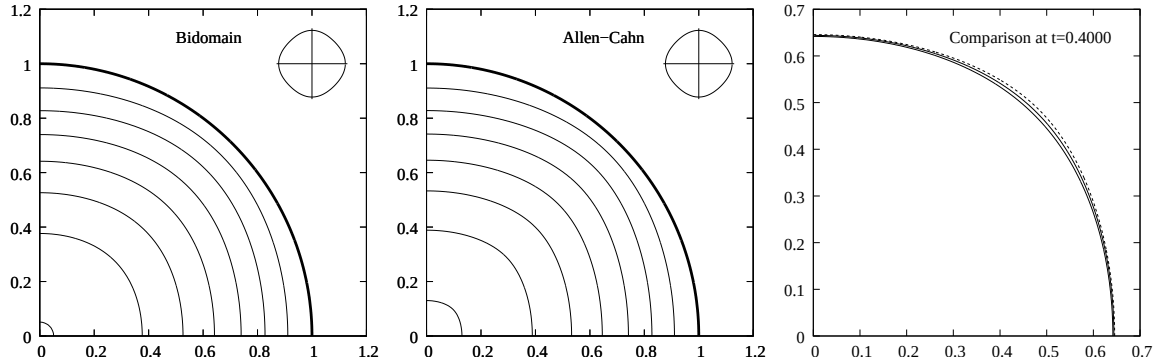

Figure 4: Simulation with $\rho = 2$, $\epsilon = 0.08$, $h = 0.01$ at time steps intervals of 0.1. Bidomain problem (left); anisotropic Allen-Cahn (middle); comparison at $t = 0.4$ between Allen-Cahn (dashed line) and bidomain with $\epsilon = 0.04$, $h = 0.005$ and with $\epsilon = 0.08$, $h = 0.01$ (solid lines), (right).

with γ given by (3.22), whereas the Dirichlet boundary data for u_ϵ^{i} and u_ϵ^{e} are respectively $\pm\frac{1}{2}$ of the initial datum along the right and top sides of the domain, with homogeneous Neumann condition along the coordinate axes.

We then select the value $\epsilon = 0.04$ and solve numerically the bidomain problem with a space discretization $h = 0.005$ and a time step suitably chosen so as to ensure stability ($\tau = Ch^2$). The resulting stiffness matrices have dimension 40000×40000. Figure 3 (left) shows the zero-level sets of the computed difference $u_\epsilon^{\mathrm{i}} - u_\epsilon^{\mathrm{e}}$ at time intervals of 0.1; it vanishes approximately at time 0.4975 that should be compared to the value 0.5 for the sharp interface limit with a relative error of less that 0.005.

A comparison with the exact sharp interface limit (anisotropic curvature flow) is shown in Figure 3 (right) at time $t = 0.3$: the dotted line is the expected sharp interface limit (rescaled Wulff shape).

A second simulation is shown in Figure 4. Now the initial datum is the unit circle (actually, the initial datum for $u_\epsilon^{\mathrm{i}} - u_\epsilon^{\mathrm{e}}$ is chosen so that its zero-level set is the unit circle), the domain is the square $(0, 1.2) \times (0, 1.2)$. We do not have the exact sharp limit evolution, so that we compare the resulting numerical solution with the numerical evolution of the anisotropic Allen-Cahn

equation with the choice φ^o as anisotropy and with corresponding initial datum. It is known that the anisotropic Allen-Cahn equation produces a zero-level set that approximates with an $\mathcal{O}(\epsilon^2)$ error the corresponding anisotropic curvature flow.
Figure 4 compares the above-mentioned anisotropic Allen-Cahn evolution (middle picture) end the bidomain numerical solution (left picture) with $\epsilon = 0.08$ (and $h = 0.01$). It is apparent that the bidomain evolution has the tendency to overly smooth out those regions of the front that correspond to higher (euclidean) curvature of the Wulff shape, this was also apparent in the simulation shown in Figure 3. Such behaviour could imply a limit evolution as $\epsilon \to 0$ different from that predicted by the forma asymptotics. Figure 4 (right) however clarifies the issue by comparing at a fidex time $t = 0.4$ two bidomain simulations with value of ϵ differing of a factor 2, with the anisotropic Allen-Cahn. This comparison is perfectly consistent with the formal asymptotics and also suggests that the error between the front and the limit evolution should not be expected to be better that $\mathcal{O}(\epsilon)$.

6.2 Selection of h versus ϵ

An important issue is the choice of the space discretization h. For a fixed ϵ it is expected that the discrete approximation converges to the continuous problem as $h \to 0$. We cannot expect however a good result if h is not sufficiently smaller than ϵ, since in that case we would have few nodes across the interfacial region and it will not be resolved with sufficient accuracy. For the problem at hand the *thickness* of the interface depends on the choice of the matrices M^{i} and M^{e} and on the orientation of the front, if we rely on the formal asymptotics. Note that althought the shape of the interfacial front is fixed, at first order, and given by γ (3.22), the rescaling is done in terms of d_ϵ, which in turn depends on $\varphi^o(\nabla d_\epsilon)$. It is usually understood that for similar problems that exhibit thin diffused interfaces, a number of nodes across the interface between 10 and 20 is enough to obtain reliable results, although the issue is not completely settled.
Actually, however, we cannot take h very small due to the resulting prohibitive computational cost, and this is particularly true for the simulations with larger inverted anisotropic ratio such those of Section 6.3. We are then forced to use values of h in a "dangerous" range, which produces results that could be far from accurate. This issue will be further commented in the next Section, see also Figure 10 for a visual feedback of the matter.

6.3 Simulations with $\rho = 5$

The second set of simulations is obtained with an inverted ratio of $\rho = 5$ as defined in (6.1). The combined anisotropy Φ in this case is nonconvex; its unit ball (Frank diagram) is star-shaped with respect to the origin and nonconvex (solid line in Figure 2, right). By applying the so-called Wulff construction we can still define an analogue of the Wulff shape (dashed line in Figure 2, right) which now presents swallowtails as a result of the nonconvex portions of the Frank diagram. The Wulff construction basically amounts in computing T^o on the vectors of the boundary of the Frank diagram F_φ. In the nonconvex case, the set $T^o(\partial F_\varphi)$ is no longer the boundary of a convex set (the Wulff shape) and consists of a curve (if $d = 2$) with selfintersections and cusps. Convexification of Φ produces a Wulff shape with the swallowtails cut off.

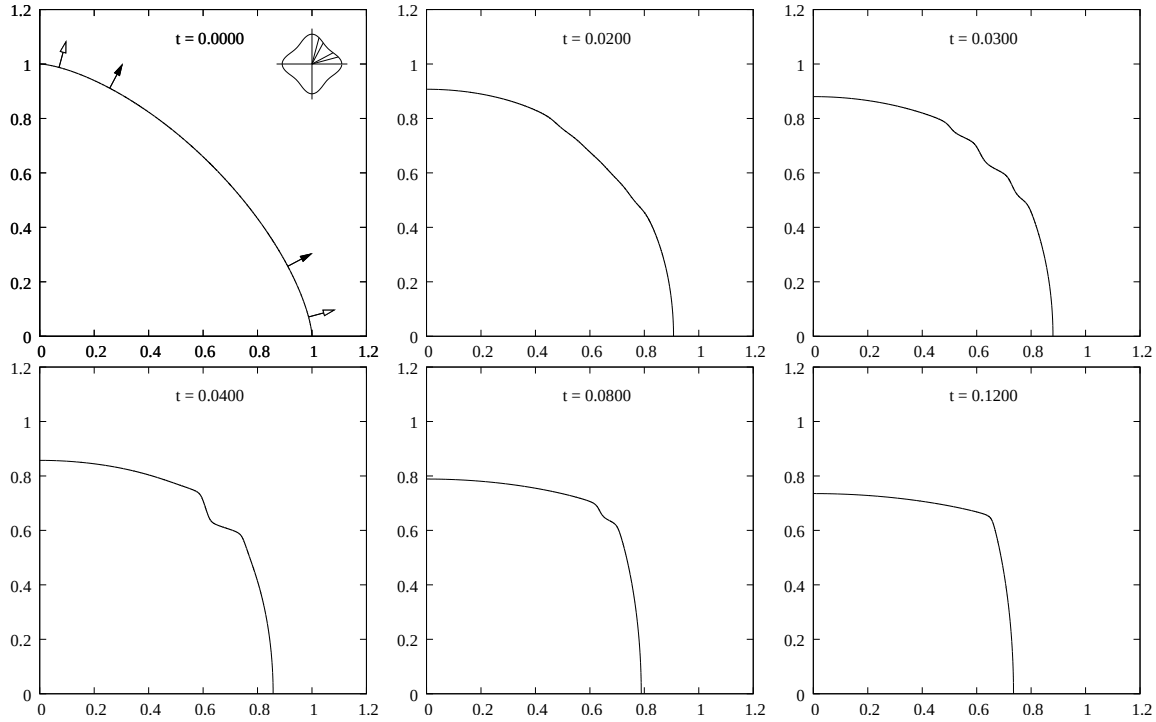

Figure 5: Simulation with $\rho = 5$, $\epsilon = 0.008$, $h = 0.002$ at different time steps.

Figure 5 shows the result of the simulation with a choice of $\epsilon = 0.008$. The initial datum is specially chosen in order to have large portions of the initial front with a normal in the concave region of the combined anisotropy. Specifically we select it such that its zero-level curve is the unit ball with respect to the $p = 1.5$ norm: $|x_1|^{1.5} + |x_2|^{1.5} = 1$. The black arrows in the first picture of Figure 5 enclose the portion of the initial front that corresponds to locally concave combined anisotropy Φ; the white arrows delimit that portion where the euclidean normal $\xi^\star$ is such that $\Phi(\xi^\star)$ is strictly larger than the convexified value (the Frank diagram lies locally inside its convex hull). The discretization parameter is fixed as $h = 0.002$, i.e. one fourth of ϵ. We are not able at present to decrease h below this value because it results into a prohibitively heavy computation.

Nonconvexity of Φ leads to an illposed anisotropic mean curvature flow. Indeed we observe at time $t = 0.02$ the formation of oscillations along the interface that later evolve into three waves with roughly flat sides whose normals approximately correspond to the two contact points between the boundary of the Frank diagram and one of the four bitangent lines. This is hardly surprising, since the corresponding slopes are the most energetically convenient.

Figures 6 and 7 shows the evolution obtained with a smaller value $\epsilon = 0.004$ ($h = 0.002$, it could not be decreased with respect to the previous simulation due to computational issues), starting with the same initial datum.

Again we see wrinkling formation starting at time $t = 0.005$. As soon as the interface starts to oscillate at some place, the oscillating region propagates very quickly into the whole *locally unstable* region (points of the front where the normal correspond to locally concave parts of the Frank diagram). Whether they also propagate in regions where the

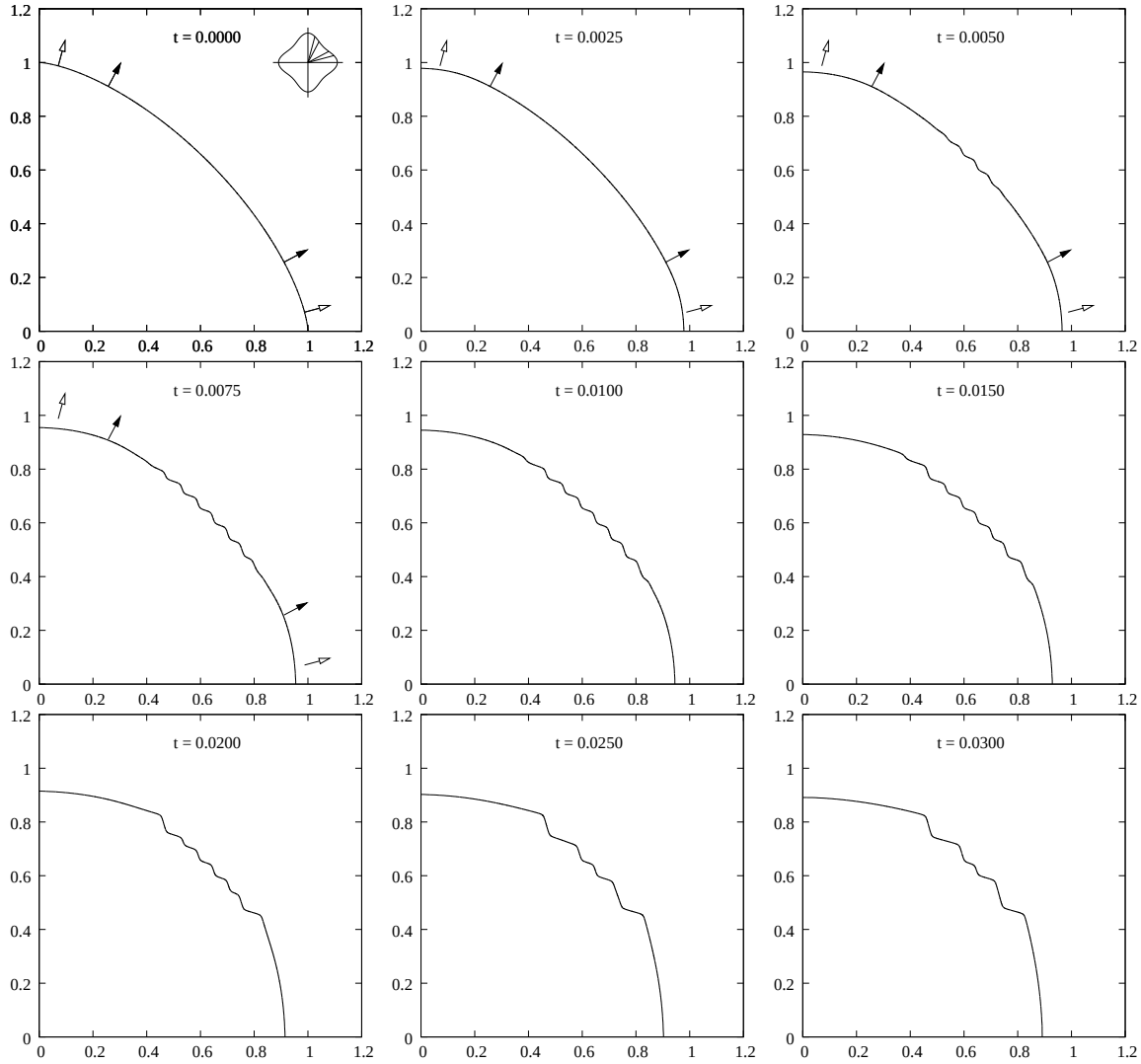

Figure 6: Simulation with $\rho = 5$, $\epsilon = 0.004$, $h = 0.002$ at different time steps. The black arrows are normals to the initial front corresponding to inflection points of the Frank diagram; the empty arrows are normals to the initial front corresponding to bitangent points of the Frank diagram.

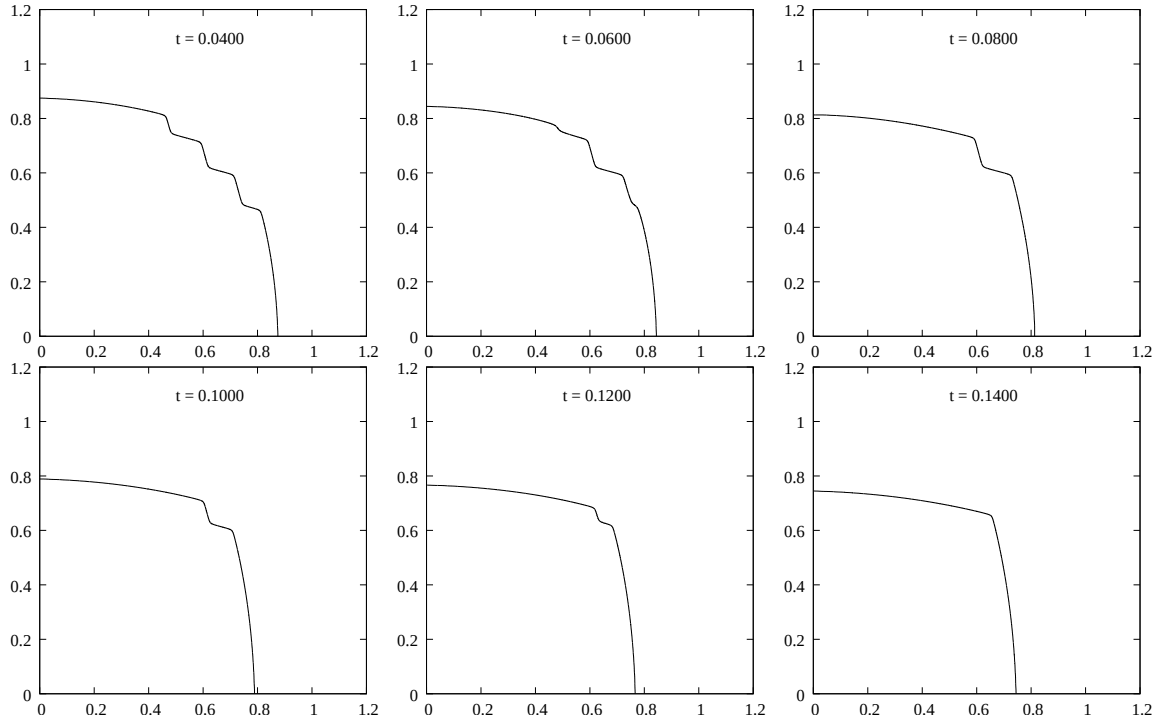

Figure 7: Simulation with $\rho = 5$, $\epsilon = 0.004$, $h = 0.002$. Subsequent times.

normal to the front correspond to locally convex, but strictly internal to the convex hull, parts of the Frank diagram is difficult to say due to the global motion of the front during the time of wrinkle formation. It is the opinion of the authors that this is not the case, which is a behaviour somewhat similar to that observed in [19] and [4] where equation of forward/backward parabolic type are relaxed either by numerical discretization or by addition of a small higher-order term. A short animation of the evolution of the front can be downloaded from `http://dmf.unicatt.it/~paolini/research/bidomain/`.

Comparing the evolutions with the two values of ϵ indicates that the wavelength of the oscillation depends linearly on ϵ with a somewhat large constant of proportionality of approximately 20 that may depend on the specific shape of the anisotropy as well as nonlocal data that can dictate the local shape of the potentials u_ϵ^{i} and u_ϵ^{e} separately.

Since the wavelength of the wrinkling decreases with $\epsilon \to 0$ one is lead to interpret the oscillating region as an approximation of a limit evolution where the limit front is thought as a kind of Young measure, i.e. a (smooth) curve with a hidden microstructure consisting of infinitesimal wrinkles that mix together two different slopes. Anisotropic curvature flows in situations where the Frank diagram presents flat portions, which is tipical of the result of convexification, have the property that the portions of the evolving curve having normals that fall inside such flat portions have zero anisotropic mean curvature, and hence to not move. They tend to disappear during evolution because they are eroded by the surrounding evolving parts. Our approximating wrinkled evolutions would be consistent with a limit anisotropic curvature flow with the convexified anisotropy *provided* that the wrinkled portion covers the *whole* globally unstable parts of the Frank diagram, i.e. those that are strictly inside the

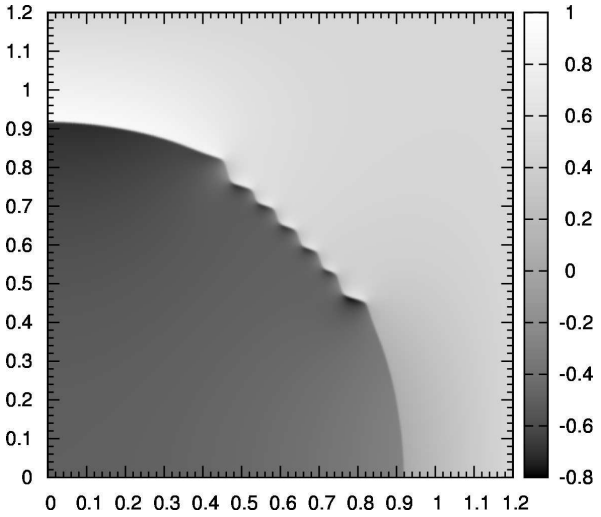

Figure 8: Simulation with $\rho = 5$, $\epsilon = 0.004$, $h = 0.002$. Plot of u^{e} at time 0.018.

convexification.

This is not the case if the oscillating portion appears only where the normal stays in the *locally* unstable part of the Frank diagram, i.e. that where the Frank diagram is concave, as apparently suggested by our simulations.

The values of u^{e}_ϵ at a fixed time $t = 0.018$ are shown in Figure 8 as grey levels.

In Figure 9 we can see a cross-section of functions u^{i}_ϵ and u^{e}_ϵ at the indicated time. The oblique line in the left picture shows the position where the cross-sections of u^{i}_ϵ (middle picture) and u^{e}_ϵ (right picture) are taken. A visual measurement allows to evaluate the normal ν at the interface in its intersection with the section line as forming an angle θ of approximately 78.1 degrees. We can then compute the corresponding values of $\alpha^{\mathrm{i}}(\nu_\varphi)$ and $\alpha^{\mathrm{e}}(\nu_\varphi)$ where $\nu_\varphi = \frac{\nu}{\varphi^o(\nu)}$ corresponds to ∇d_ϵ of section 3 using the formulas

$$\alpha^{\mathrm{i}}(\nu_\varphi) = 1 + \frac{\alpha^{\mathrm{i}}(\nu)}{\alpha^{\mathrm{e}}(\nu)} = \frac{6}{5\cos^2\theta + \sin^2\theta}, \qquad \alpha^{\mathrm{e}}(\nu_\varphi) = 1 + \frac{\alpha^{\mathrm{e}}(\nu)}{\alpha^{\mathrm{i}}(\nu)} = \frac{6}{\cos^2\theta + 5\sin^2\theta}$$

This allows to compare the theoretical value of the jump $[\![u^{\mathrm{i}}_\epsilon]\!] \approx \frac{2}{\alpha^{\mathrm{i}}} \approx 0.39$ (resp. $[\![u^{\mathrm{e}}_\epsilon]\!] \approx \frac{2}{\alpha^{\mathrm{e}}} \approx 1.61$) in the limit $\epsilon \to 0$ as given by the formal asymptotics, see (3.33), with the experimental values measured in Figure 9 that amounts to approximately 0.41 (resp. 1.59) with good agreement with the theoretical values.

We conclude by bringing up again the issue of the front resolution by taking h sufficiently small with respect to ϵ. Unfortunately the wrinkling phenomenon is only apparent if ϵ is quite small, which would force to select values for h prohibitively small. In our simulations (particularly that with the smaller ϵ, Figure 6) the value of h is actually quite large with respect to ϵ particularly in view of the somewhat extreme choice of the anisotropy.

In order to try to understand the effect of such large choice of h, Figure 10 compares the numerical simulation with two different values of h ($h = 0.004$ and $h = 0.002$) and the same value of $\epsilon = 0.008$. The difference is small in the regularly evolving parts of the front, but are quite noticeable in the wrinkled part. However the size and shape of the oscillations is

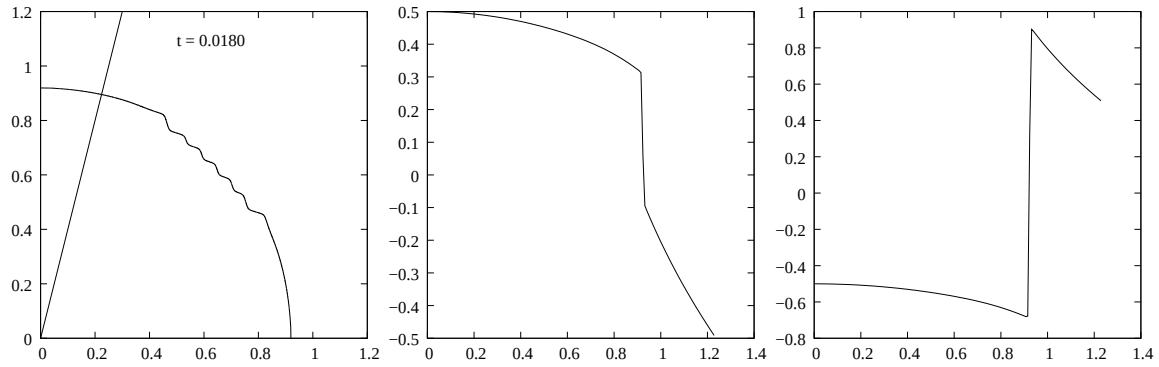

Figure 9: Section of u^{i} and of u^{e} at time 0.018.

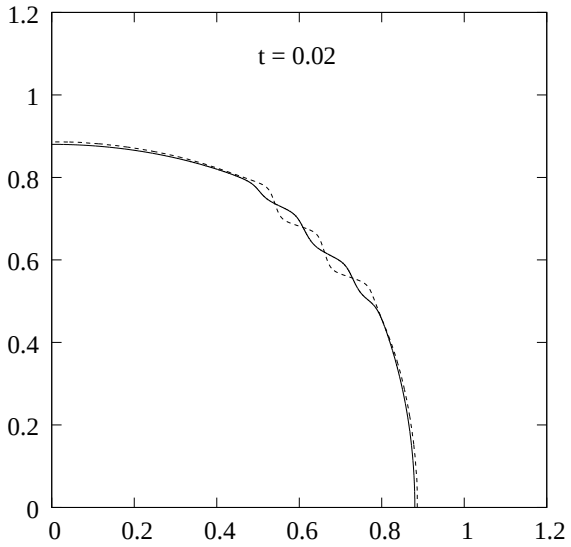

Figure 10: Comparison between $h = 0.002$ (solid line) and $h = 0.004$ (dashed line) at time $t = 0.03$ with $\rho = 5$ and $\epsilon = 0.008$.

basically the same so that we have a similar qualitative behaviour of the evolution. It seems that larger values of h also result into a more easy wrinkle formation, which tend to appear sooner during the evolution when compared to simulations with smaller values of h.
We thus conclude that although the presented simulations should not be considered particularly quantitatively accurate, nevertheless they show the correct behaviour of the continuous problem.

References

[1] L. Ambrosio, P. Colli Franzone, G. Savaré, *On the asymptotic behaviour of anisotropic energies arising in the cardiac bidomain model*, Interfaces and Free Boundaries, **2** (2000), 213–266.

[2] D. Bao, S.-S. Chern, Z. Shen, *An introduction to Riemann-Finsler Geometry*, Graduate Texts in Mathematics, 200. Springer-Verlag, 2000.

[3] G. Bellettini, P. Colli Franzone, M. Paolini, *Convergence of front propagation for anisotropic bistable reaction–diffusion equations*, Asymptotic Anal., **15** (1997), 325–358.

[4] G. Bellettini, G. Fusco, N. Guglielmi, *A concept of solution and numerical experiments for forward-backward diffusion equations of the form* $u_t = \frac{1}{2}(\phi'(u_x))_x$ *and numerical experiments for the singular perturbation* , $u_t = -\epsilon^2 u_{xxxx} + \frac{1}{2}(\phi'(u_x))_x$, Discrete Contin. Dyn. Syst. **16** (2006), 783–842.

[5] G. Bellettini, C. Mantegazza, M. Novaga, *Singular perturbations of mean curvature flow*, J. Differential Geom. **57** (2007), 403–431.

[6] G. Bellettini, M. Novaga, M. Paolini, *Facet-breaking for three-dimensional crystals evolving by mean curvature*, Interfaces Free Bound. **1** (1999), 39-55.

[7] G. Bellettini, M. Novaga, M. Paolini, *On a crystalline variational problem, part I: first variation and global* L^∞*-regularity* Arch. Ration. Mech. Anal. **157** (2001), 165-191.

[8] G. Bellettini, M. Novaga, M. Paolini, *On a crystalline variational problem, part II: BV-regularity and structure of minimizers on facets*, Arch. Ration. Mech. Anal. **157** (2001) 3, 193-217.

[9] G. Bellettini, M. Paolini, *Quasi-optimal error estimates for the mean curvature flow with a forcing term*, Differential Integral Equations **8** (1995), 735–752.

[10] G. Bellettini, M. Paolini, *Anisotropic motion by mean curvature in the context of Finsler geometry*, Hokkaido Math. J., **25** (1996), 537–566.

[11] G. Bellettini, M. Paolini, S. Venturini: *Some results on surface measures in Calculus of Variations*, Ann. Mat. Pura Appl. **CLXX** (1996), 329–359.

[12] K. A. Brakke, *The Motion of a Surface by its Mean Curvature*, Math. Notes 20, Princeton University Press, 1978,

[13] P.G. Ciarlet, *The Finite Element Method for Elliptic Problems*, North-Holland, Amsterdam, 1978.

[14] P. Colli Franzone, M. Pennacchio, G. Savaré, *Multiscale modeling for the bioelectric activity of the heart*, SIAM J. Math. Anal. **37** (2005), 1333–1370.

[15] P. Colli Franzone, G. Savaré, *Degenerate evolution systems modeling the cardiac electric field ad micro and macroscopic level*, Evolution equations, semigroups and functional analysis (Milano 2000), vol. 50, Progress Nonlin. Diff. Equations Appl. Birkhäuser, Basel (2002), 49–78.

[16] E. De Giorgi, *Congetture riguardanti alcuni problemi di evoluzione*, Duke Math. J. **81** (1995), 255-268

[17] K. Ecker: *Regularity Theory for Mean Curvature Flow*, Progress in Nonlinear Differential Equations and their Applications, 57, Birkäuser, Boston, MA, 2004.

[18] L.C. Evans, M. Portilheiro, *Irreversibility and hysteresis for a forward-backward diffusion equation*, Math. Models Methods Appl. Sci. **LIV** (2004), 1599–1620.

[19] F. Fierro, R. Goglione, M. Paolini, *Numerical simulations of mean curvature flow in presence of a nonconvex anisotropy*, Math. Models Methods Appl. Sci. **4** (1998), 573–601.

[20] T. Fukui, Y. Giga, *Motion of a graph by nonsmooth weighted curvature*, World Congress of Nonlinear Analysts '92, Vol. I-IV (1996), 47-56.

[21] M. Gage, R.S. Hamilton, *The heat equation shrinking convex plane curves*, J. Differential Geom. **23** (1986), 69-96.

[22] Y. Giga, *Surface Evolution Equations. A Level Set Approach*, Monographs in Mathematics, **99**, Birkhäuser, Basel, 2006.

[23] M. H. Giga, Y. Giga, *Evolving graphs by singular weighted curvature*, Arch. Ration. Mach. Anal. **141** (1998), 117-198.

[24] M. H. Giga, Y. Giga, *Stability for evolving graphs by nonlocal weighted curvature*, Comm. Partial Differential Equations **24** (1999), 109-184.

[25] Y. Giga, S. Goto, *Geometric evolutions of phase-boundaries,* On the Evolution of Phase-Boundaries (M. Gurtin and Mc Fadden, eds.), IMA Vols. Math. Appl. vol. 43, Springer-Verlag, Berlin (1992), 51-66.

[26] Y. Giga, M. Paolini, P. Rybka, *On the motion by singular interfacial energy*, Japan J. Indust. Appl. Math. **18** (2001), 47–64.

[27] A.L. Hodgkin, A.F. Huxley, *A quantitative description of membrane current and its application to conduction and excitation in nerve*, J. Physiol. **117** (1952), 500–544.

[28] G. Huisken, *Flow by mean curvature of convex surfaces into spheres*, J. Differential Geom. **20** (1984), 237–266.

[29] G. Huisken, *Asymptotic behaviour for singularities of the mean curvature flow*, J. Differential Geom. **31** (1990), 285–299.

[30] G. Huisken, *Local and global behaviour of hypersurfaces moving by mean curvature*, Proc. of Symp. Pure Math., **54** (1993), 175–191.

[31] C. Mantegazza. *Lecture Notes on Mean Curvature Flow*, Progress in Math. 290, Birkhäuser, 2011.

[32] R.M. Miura, *Accurate computation of the stable solitary wave for the FitzHugh-Nagumo equations*, J. Math. Biol. **13** (1981/82), 247–269.

[33] M. Paolini, F. Pasquarelli, *Numerical simulation of crystalline curvature flow in 3D by interface diffusion*, Free Boundary Problems: theory and applications II, GAKUTO Internat. Ser. Math. Sci. Appl. 14 (N. Kenmochi ed.), Gakkötosho, Tokyo (2000), 376–389.

[34] M. Paolini, C. Verdi, *Asymptotic and numerical analyses of the mean curvature flow with a space-dependent relaxation parameter*, Asymp. Anal. **5** (1992), 553–574.

[35] P.I. Plotnikov, *Passage to the limit with respect to viscosity in an equation with variable parabolicity direction*, Differential Equations **30** (1994), 614–622.

[36] M. Slemrod, *Dynamics of measured valued solutions to a backward-forward heat equation*, J. Dyn. Differential Equations **3** (1991), 614–622.

[37] F. Smarrazzo, A. Tesei, *Degenerate regularization of forward-backward parabolic equations. Part I: the regularized problem*, Arch. Rat. Mech. Anal. (to appear).

[38] J. E. Taylor, *Motion by crystalline curvature*, in Computing Optimal Geometries, Jean E. Taylor, ed., Selected Lectures in Mathematics, Amer. Math. Soc. (1991), 63-65, and accompanying video.

[39] J.E. Taylor, *II-Mean curvature and weighted mean curvature,* Acta Metall. Mater. **40** (1992), 1475-1485.

[40] J. E. Taylor, *Motion of curves by crystalline curvature, including triple junctions and boundary points*, Differential Geometry, Proc. Sympos. Pure Math. **54** (part 1) (1993), 417-438.